

International Journal of Modern Physics A
 © World Scientific Publishing Company

SIGNATURES OF SINGLET NEUTRINOS IN LARGE EXTRA DIMENSIONS AT THE LHC

DOUGLAS M. GINGRICH*

*Centre for Particle Physics, Department of Physics,
 University of Alberta, Edmonton, AB T6G 2G7 Canada
 gingrich@ualberta.ca*

Received 10 July 2009
 Revised 27 August 2009

It is a challenge to explain why neutrinos are so light compared to other leptons. Small neutrino masses can be explained if right-handed fermions propagate in large extra dimensions. Fermions propagating in the bulk would have implications on Higgs boson decays. If the Higgs boson is discovered at the Large Hadron Collider (LHC), a detailed analysis may reveal the presence of large extra dimensions. This paper reviews the status of large extra-dimensional models in the context of the current limits on Higgs boson masses and the fundamental Planck scale in extra dimensions.

Keywords: neutrinos; extra dimensions; beyond Standard Model

1. Introduction

Neutrino oscillation experiments suggest that neutrinos have a very small but nonzero mass.^{1–11} To explain why neutrinos are so light compared to other leptons is a challenge. The traditional approach is to give neutrinos small mass via a seesaw mechanism. In the type-I seesaw approach, a large right-handed Majorana mass M_R suppresses one of the eigenvalues of the neutrino mass matrix. This leads to a neutrino mass $m_\nu \sim m_D^2/M_R$, where m_D is the mass of a light Dirac fermion. The neutrino mixing required to explain the atmospheric, solar, and accelerator neutrino oscillation data requires a super-heavy energy scale for M_R . Explaining the neutrino masses and oscillations is one of the grand challenges of particle physics.

Another interesting challenge is to explain the hierarchy problem: the fine tuning required to maintain a low electroweak scale in the presence of the Planck scale. Supersymmetry, technicolour, and extra dimensions have all been used to address the hierarchy problem. In particular, the extra-dimensions paradigm can lead to the possibility of low-scale gravity.^{12–14} In the large extra-dimensions approach (often referred to as ADD), the Standard Model (SM) fields are usually localised on (3+1)-dimensional wall (a 3-brane), while gravity is allowed to propagate in all

*Also at TRIUMF, Vancouver, BC V6T 2A3 Canada

2 *Douglas M. Gingrich*

of the dimensions (the bulk). If the fundamental gravity scale is about a TeV, the ultraviolet cut-off for quantum corrections to the Higgs boson mass is also about a TeV. This recasts the hierarchy problem in terms of geometry and the stabilisation of large extra dimensions.

In the large extra-dimensions paradigm, small neutrino masses can be generated without implementing a super-heavy energy scale, as done in a seesaw mechanism^a. Small neutrino masses are naturally explained if at least one right-handed fermion propagates in the extra dimensions.^{15–17} Since the SM gauge fields are localised to the 3-brane, a bulk fermion must be a SM singlet: “bulk right-handed neutrino” or “singlet right-handed neutrino”. Right-handed neutrinos can freely propagate in the extra dimensions because they have no quantum numbers to constrain them to the SM 3-brane. Therefore, they can also be classified as “sterile” neutrinos. The bulk neutrinos couple to the brane-localised SM fields with small Yukawa couplings. The couplings are small because of the large relative volume of the bulk manifold compared to the thin SM 3-brane. However, because of mixing with a large number of Kaluza Klein (KK) states in the bulk, the interaction probability with the SM fields can be enhanced. Thus the effect of bulk neutrinos on, for example, Higgs boson decays can be significant.

This paper is organised as follows. Section 2 considers some of the experimental results from neutrino experiments that we will use. Section 3 reviews the ideas of right-handed neutrinos in large extra dimensions. The neutrino mass and coupling are discussed in subsection 3.1 and subsection 3.2, respectively. Subsection 3.3 presents bulk neutrinos in other spaces and the effect of compactification. Constraints on the size and number of extra dimensions are discussed in subsection 3.4. Section 4 identifies some of the signatures of right-handed neutrinos in large extra dimensions, which could be revealed by experiments at the LHC. First examined are the implications for the τ lepton decay of a heavy charged Higgs boson in subsection 4.1. Then, the invisible decay mode of a light Higgs boson is explored in subsection 4.2. Finally, section 5 summarises our findings. With the startup of the LHC, such detailed phenomenological reviews are timely and of value.

2. Some Neutrino Oscillation and Mass Results

Nearly all the useful measurements of neutrino properties, that we will be concerned with, come from neutrino flavour oscillation experiments. Neutrino oscillations imply that the neutrinos have mass and that their lepton flavour is mixed. From neutrino oscillation experiments, one can deduce the absolute difference in the square of neutrino masses. It is common to associate measurements from solar neutrino oscillation experiments with $\Delta m_{\odot}^2 = \Delta_{21}^2 = m_2^2 - m_1^2$ and $\theta_{\odot} = \theta_{12}$, and measurements from atmospheric neutrino experiments with $\Delta m_{\text{atm}}^2 = \Delta_{32}^2 = |m_3^2 - m_2^2|$ and $\theta_{\text{atm}} = \theta_{23}$, where m_1, m_2 , and m_3 are the neutrino physical masses. The

^aHigher-dimensional seesaw mechanisms are also possible.¹⁵

LSND results¹⁸ are not considered in this paper. These results have been shown to be incompatible with solar and atmospheric oscillation data in models of bulk neutrinos.¹⁹

The experimental oscillation measurements lead to the following results, which are summarised by the Particle Data Group.²⁰ The current values from solar neutrinos are

$$\Delta m_{21}^2 = (8.0 \pm 0.3) \times 10^{-5} \text{ eV}^2 \quad \text{and} \quad \sin^2(2\theta_{12}) = 0.86_{-0.04}^{+0.03} \quad (1)$$

at the 68% confidence level. The current bounds from atmospheric neutrinos are

$$\Delta m_{32}^2 = (1.9 \text{ to } 3.0) \times 10^{-3} \text{ eV}^2 \quad \text{and} \quad \sin^2(2\theta_{23}) > 0.92 \quad (2)$$

at the 90% confidence level. The best fit is $\Delta m_{32}^2 = 2.4 \times 10^{-3} \text{ eV}^2$. Only a bound is known on the third angle $\sin^2(2\theta_{13}) < 0.19$.

The mass-squared differences can be accommodated within the SM of three active neutrino flavours ν_e , ν_μ , and ν_τ . Since only the absolute difference of the squares of masses has been determined in atmospheric neutrino oscillation experiments, the order of the masses is not known. Possible mass hierarchies are shown in Fig. 1. For the normal and inverted hierarchies, we typically assume $\Delta m_{\text{atm}}^2 = \Delta m_{32}^2 \sim \Delta m_{31}^2$.

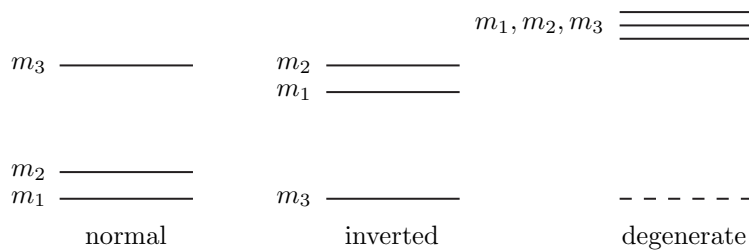


Fig. 1. Possible neutrino mass hierarchies.

For the normal and inverted mass hierarchies, the values of m_1 , m_2 , and m_3 are assumed to be of the same order of magnitude as the larger of the mass differences. For the normal mass hierarchy, $m_1 = 0$ and $m_3 \gg m_2$ is usually assumed. This leads to $m_3 = \sqrt{\Delta m_{\text{atm}}^2} \approx 0.05 \text{ eV}$ and $m_2 = \sqrt{\Delta m_{\odot}^2} \approx 0.009 \text{ eV}$. For the inverted mass hierarchy, $m_3 = 0$ and $m_1 \approx m_2$ is usually assumed. This leads to $m_1 = m_2 = \sqrt{\Delta m_{\text{atm}}^2} \approx 0.05 \text{ eV}$. In the degenerate mass scheme, $m_1 = m_2 = m_3 \approx 1 \text{ eV}$ is a common arbitrary choice.

Current cosmological data and some cosmological assumptions suggest that²⁰

4 *Douglas M. Gingrich*

$$\sum_i m_i < (0.17 - 2.0) \text{ eV}. \quad (3)$$

Here the sum is over neutrino states that were in thermal equilibrium in the early universe. The mass of the heaviest neutrino is bounded by²⁰

$$0.04 \text{ eV} < m_{\text{heaviest}} < (0.07 - 0.7) \text{ eV}, \quad (4)$$

where the lower bound is because the mass of the heaviest neutrino cannot be lighter than $\sqrt{\Delta m_{\text{atm}}^2}$. This suggests that a more reasonable value to choose for the neutrino mass in the degenerate scheme is 0.7 eV.

3. Right-Handed Neutrinos in Large Extra Dimensions

In this section, we review the aspects of neutrinos in large extra dimensions that will be needed to discuss their effects on Higgs bosons. The ansatz of the large extra dimension paradigm is encompassed in the following relationship.

$$\bar{M}_{\text{Pl}}^2 = \bar{M}_D^{2+\delta} V_\delta = M_D^{2+\delta} R^\delta, \quad (5)$$

where $\bar{M}_{\text{Pl}} = 1/\sqrt{8\pi G_N} \approx 2.4 \times 10^{18}$ GeV is the reduced 4-dimensional Planck scale, δ is the number of additional spatial dimensions, M_D is the fundamental Planck scale of gravity in $(4 + \delta)$ -spacetime dimensions, and $V_\delta = L_1, \dots, L_\delta$ is the volume of the compact extra-dimensional space (where L_i is the size of the i th compact dimension). Assuming the volume has the configuration of a torus, $L_i = 2\pi R_i$. In the simple case where all of the compact extra dimensions have equal radii R , $V_\delta = (2\pi R)^\delta$. The case of non-equal radii and configurations other than a torus will be discussed in section 3.4.

Throughout this paper, M_D is used as the definition of the fundamental Planck scale linking experimental measurements to the theory. In the literature on bulk neutrinos in large extra dimensions, it is common to use M_* defined by $\bar{M}_{\text{Pl}}^2 = M_*^{2+\delta} R^\delta$, and consider R^δ as the volume in δ -dimensional space.

Limits on M_D and R have been set by direct gravity measurements, experiments at accelerators, and constraints from astrophysics and cosmology. The Eöt-Washington group constrained the size of the largest extra dimension to $R < 44 \mu\text{m}$ at the 95% confidence level.²¹ This completely rules out TeV-scale gravity with one large extra dimension. For two large extra dimensions, they obtain $R < 30 \mu\text{m}$.²⁰ The sensitivity to three or more extra dimensions of equal size is only weakly constrained by accelerator experiments. For $\delta = 3$, M_D is greater than 1.2 TeV and for $\delta = 4$, M_D is greater than 0.94 TeV from the LEP experiments. For $5 \leq \delta \leq 8$, M_D is greater than 0.8 TeV from the Tevatron experiments. The astrophysical and cosmological limits on M_D are high, particularly for two or three extra dimensions. However, they are based on a number of assumptions so the results are only order

of magnitude estimates. Thus, we will not consider further astrophysical or cosmological limits. We will often be interested in the quantity $1/R$. The best limits on $1/R$ based on the numbers above are $1/R > 7 \times 10^{-3}$ eV for $\delta = 2$, $1/R > 75$ eV for $\delta = 3$, and $1/R > 2 \times 10^4$ eV for $\delta = 4$.

When adding a right-handed neutrino to the paradigm of large extra dimensions, there are two common approaches taken. One approach is to introduce a separate bulk fermion for each flavour of neutrino on the SM brane.^{16,22} This approach extends the concept of flavour into the bulk. A second approach is to introduce only one bulk fermion and give this fermion a flavour-universal coupling to all three SM brane neutrinos.^{23,24} In this approach, flavour is a feature internal to the SM and is restricted to the SM brane. For simplicity of illustration, we will consider a model of three separate bulk neutrinos.

We can view the Lagrangian density as split into separate bulk and SM brane contributions. The action can be written as

$$S = \int d^4x d^\delta y [\mathcal{L}_{\text{bulk}} + \delta(\vec{y})\mathcal{L}_{\text{brane}}] , \quad (6)$$

where $\mathcal{L}_{\text{brane}}$ contains the usual SM Lagrangian plus the interaction terms with the bulk fields, while $\mathcal{L}_{\text{bulk}}$ contains the dynamical terms for the bulk fields and the usual Einstein-Hilbert gravity term. The extra δ -dimensions are represented by the coordinates $\vec{y} = (y^1, \dots, y^\delta)$. Since we will only be considering thin SM branes, we use the delta function $\delta(\vec{y})$ to precisely locate the SM fields and connect the fields on the two manifolds. Small spreading from $y = 0$, such as in models of split fermions, have also been considered.²⁵

To further simplify things, we will consider a 5-dimensional theory. In addition, a theory of more than one extra dimension approximates to the 5-dimensional theory when one of the extra dimensions is much larger than the sizes of the other dimensions. The generalisation to more than one extra dimension is straight forward except for one non-trivial detail. This is how the higher-dimensional spinor in the bulk couples to the lepton spinor on the 3-brane. For a generalisation of the 6-dimensional case see Ref. 26.

We begin by adding Dirac fermions to the bulk with wave function $\Psi^\alpha(x^\mu, \vec{y})$, where $\alpha = 1, 2$, and 3 is the flavour index. In the 4-dimensional Weyl basis, a 4-component Dirac spinor can be decomposed as

$$\Psi^\alpha(x^\mu, \vec{y}) = \begin{bmatrix} \psi_L^\alpha(x^\mu, \vec{y}) \\ \psi_R^\alpha(x^\mu, \vec{y}) \end{bmatrix} , \quad (7)$$

where ψ_L^α and ψ_R^α are 2-component complex Weyl spinors. The L and R subscripts explicitly indicate the 4-dimensional Lorentz property. For the next little while, the flavour index is omitted to simplify the notation.

The 5-dimensional coordinates are $x^A \equiv (x^\mu, y)$, where x^μ are not compactified and y is a single coordinate perpendicular to the brane. The y -direction is com-

6 *Douglas M. Gingrich*

pactified on a circle of circumference $2\pi R$ by making the periodic identification $y \sim y + 2\pi R$. On the 3-brane $y = 0$.

In the Weyl basis, the 5-dimensional Dirac matrices Γ have size 4×4 and can be written as

$$\Gamma^\mu = \begin{pmatrix} 0 & \sigma^\mu \\ \bar{\sigma}^\mu & 0 \end{pmatrix} \quad \text{and} \quad \Gamma^5 = -i\gamma_5 = \begin{pmatrix} i & 0 \\ 0 & -i \end{pmatrix}, \quad (8)$$

where $\sigma^\mu = (1, \sigma^i)$ and $\bar{\sigma}^\mu = (1, -\sigma^i)$, and the σ^i are the three Pauli matrices.

The free action for bulk fermions is

$$S_{\text{bulk}} = \int d^4x dy \bar{\Psi}(x, y) i\Gamma^A \partial_A \Psi(x, y), \quad (9)$$

where

$$\bar{\Psi} = \Psi^\dagger \Gamma^0 \quad \text{and} \quad \Psi^\dagger = (\psi_L^\dagger, \psi_R^\dagger). \quad (10)$$

The bulk action in terms of 2-component spinors is

$$S_{\text{bulk}} = \int d^4x dy \left[\psi_R^\dagger i\sigma^\mu \partial_\mu \psi_R + \psi_L^\dagger i\bar{\sigma}^\mu \partial_\mu \psi_L - \psi_R^\dagger \partial_5 \psi_L + \psi_L^\dagger \partial_5 \psi_R \right]. \quad (11)$$

To obtain the 4-dimensional effective theory, it is common to compactify the large (flat) extra dimensions on a torus by making the identification $y^i \sim y^i + 2\pi R$ for each dimension. This suggests performing a KK expansion of the form

$$\psi(x^\mu, \vec{y}) = \sum_{\vec{n}} \psi^{(\vec{n})}(x^\mu) f_{\vec{n}}(\vec{y}), \quad (12)$$

where $\vec{n} = (n_1, \dots, n_\delta)$ is a vector in number space (n_i can be positive, negative, or zero), $\psi^{(\vec{n})}$ are the KK modes, and $f_{\vec{n}}(\vec{y})$ are a complete set of periodic orthogonal functions over the \vec{y} space that satisfy

$$\int_0^{2\pi R} d^\delta y f_{\vec{n}}^\dagger(\vec{y}) f_{\vec{m}}(\vec{y}) = \delta_{\vec{n}\vec{m}}. \quad (13)$$

The usual choice for $f_{\vec{n}}(\vec{y})$ that exhibits the wave nature of the wave function is

$$f_{\vec{n}}(\vec{y}) = \frac{e^{-2\pi i \vec{n} \cdot \vec{y} / (V_\delta)^{1/\delta}}}{\sqrt{V_\delta}}. \quad (14)$$

For higher-dimensional fermion fields, the KK expansion must include a higher-dimensional Weyl spinor. In the simplified 5-dimensional case considered here, the spinor is the same as the usual 4-dimensional Weyl spinor and is contained in $\psi^{(\vec{n})}$.

For higher-dimensions, $\psi^{(\vec{n})}$ must have a vector structure and the representation of the chirality multiplets is not unique.

Often Eq. (14) is used for the KK expansion and boundary conditions are imposed afterwards. Since the spectra resulting from toroidal compactification is typically not chiral, we will compactify on an orbifold $\mathcal{T}^\delta/\mathcal{Z}_2$: the quotient space of a δ -dimensional torus will inversion symmetry. When an extra space dimension is compactified under the group of \mathcal{Z}_2 isometries, it is natural for one of the 2-component Weyl spinors, e.g. ψ_R , to be taken to be even under the \mathcal{Z}_2 action $y \rightarrow -y$, while the other spinor ψ_L is taken to be odd. The left-handed SM neutrino ν_L is restricted to a brane localised at the orbifold fixed point $y = 0$, while ψ_L vanishes at this point. From the 4-dimensional point of view, a higher-dimensional SM singlet fermion can be decomposed into a tower of KK excitations

$$\psi_R(x, y) = \frac{1}{\sqrt{2\pi R}} \psi_R^{(0)}(x) + \frac{1}{\sqrt{\pi R}} \sum_{n=1}^{\infty} \psi_R^{(n)}(x) \cos\left(\frac{ny}{R}\right), \quad (15)$$

$$\psi_L(x, y) = \frac{1}{\sqrt{\pi R}} \sum_{n=1}^{\infty} \psi_L^{(n)}(x) \sin\left(\frac{ny}{R}\right), \quad (16)$$

where $\psi_{R/L}^{(n)}(x)$ are 4-dimensional states: right- and left-handed Weyl spinors. The first term of ψ_R is the zero mode and is independent of the extra dimensions. The other terms are called KK modes. We point out that ψ_L does not have a zero mode.

The 4-dimensional effective theory is obtained by substituting Eq. (15) and Eq. (16) into Eq. (11), and integrating out y (dimensional reduction) to obtain

$$S_{\text{bulk}} = \int d^4x \left[\psi_R^{(0)\dagger} i\sigma^\mu \partial_\mu \psi_R^{(0)} + \sum_{\hat{n}=1}^{\infty} \left(\psi_R^{(\hat{n})\dagger} i\sigma^\mu \partial_\mu \psi_R^{(\hat{n})} + \psi_L^{(\hat{n})\dagger} i\bar{\sigma}^\mu \partial_\mu \psi_L^{(\hat{n})} \right) - \sum_{\hat{n}=1}^{\infty} \frac{|\hat{n}|}{R} \left(\psi_R^{(\hat{n})\dagger} \psi_L^{(\hat{n})} + \psi_L^{(\hat{n})\dagger} \psi_R^{(\hat{n})} \right) \right]. \quad (17)$$

We have now generalized beyond a single extra dimension to the higher extra-dimensional case. The vector in number space now has magnitude $|\hat{n}| = \sqrt{n_1^2 + \dots + n_\delta^2}$, where n_i includes only the positive modes, but excludes the zero mode. We observe the usual tower of KK states in which the Dirac masses are $|\hat{n}|/R$. The sum over \hat{n} can in principle go to infinity, leading to an infinite tower of Dirac KK states. However, we take the view that this extra-dimensional effective field theory description is only valid up to a cut-off scale of approximately M_D and therefore truncate the sum such that the highest KK mass is below M_D . The zero mode $\psi_R^{(0)}$ decouples from the tower of KK states and is exactly massless.

In the effective 4-dimensional theory, the most general $SU(2)$ invariant expression describing the interaction between brane and bulk fields is

8 *Douglas M. Gingrich*

$$\begin{aligned}
S_{\text{int}} &= -\frac{g}{\sqrt{M_D^\delta}} \int d^4x \bar{\ell}_L(x) \phi_c(x) \psi_R(x, \vec{y}=0) + H.c. \\
&= -\frac{g}{\sqrt{M_D^\delta V_\delta}} \int d^4x \left(\nu_L^\dagger, \ell_L^\dagger \right) \begin{pmatrix} \bar{\phi}^0 \\ -\phi^- \end{pmatrix} \left[\psi_R^{(0)} + \sqrt{2} \sum_{\hat{n}=1}^{\infty} \psi_R^{(\hat{n})} \right] + H.c., \quad (18)
\end{aligned}$$

where ℓ_L is a left-handed lepton doublet, ϕ_c is the SM Higgs doublet with hypercharge -1 , and g is a dimensionless Yukawa coupling constant. The flavour indices in Eq. (18) have been suppressed. The coupling g can be made diagonal in flavour space by applying two unitary transformations (see section 3.1). The lepton doublet and Higgs field lie on the 3-brane, while the massless Dirac fermion ψ_R propagates in the full extra-dimensional space. The coupling of Eq. (18) breaks the full Poincaré invariance of the theory by picking out the component ψ_R from the full Dirac spinor Ψ . This can be expected since the presence of the wall itself breaks the higher-dimensional Poincaré transformations. The four dimensional theory is still Lorentz invariant.

One of the crucial questions in explaining neutrino masses and oscillations is the violation of lepton number. We assume lepton number is conserved and assign Ψ the opposite lepton number to the lepton doublet in Eq. (18). Since we do not include Majorana masses, the action conserves lepton number and only Dirac neutrino masses are possible for the left-handed neutrinos. There have been a number of models that combine the ideas of large extra dimensions with additional ingredients, such as, small Majorana masses for the brane neutrinos.¹⁵

The KK states do not mix with each other and the left-handed KK states do not interact with the SM fields. However, the KK states do not completely decouple from the system. The lowest-lying active neutrino (SM neutrino ν_L) will mix with the entire tower of $\psi_R^{(\hat{n})}$ states. Thus the KK states can participate in neutrino oscillations, acting effectively as a large number of sterile neutrinos.

After $SU(2)$ symmetry breaking by the Higgs mechanism,

$$\phi_c = \begin{pmatrix} \frac{v+H(x)}{\sqrt{2}} \\ 0 \end{pmatrix}. \quad (19)$$

The Higgs field acquires a vacuum expectation value (VEV) $v = (\sqrt{2}G_F)^{-1/2} = m_W/(2g_W) = 246$ GeV. The interaction term in the action becomes

$$S_{\text{int}} = -\frac{m_D}{v} \int d^4x \bar{\nu}_L H \left[\psi_R^{(0)} + \sqrt{2} \sum_{\hat{n}=1}^{\infty} \psi_R^{(\hat{n})} \right] + H.c., \quad (20)$$

where

$$m_D = \frac{gv}{\sqrt{2\bar{M}_D^\delta V_\delta}} = \frac{g}{\sqrt{2}} \frac{\bar{M}_D}{M_{\text{Pl}}} v. \quad (21)$$

Thus, we see that the interactions between the bulk fermions and the brane fields generate Dirac mass terms between the brane fields and all the KK modes of the singlet neutrinos via their Yukawa coupling to the Higgs VEV. The Yukawa couplings of the bulk fields are suppressed by the volume of extra dimensions. The last expression in Eq. (21) appears to be independent of the number of extra dimensions; the number of extra dimensions is hidden in the definition of $\bar{M}_D = M_D/(2\pi)^{\delta/(2+\delta)}$. In terms of known values

$$m_D \sim g \frac{\bar{M}_D}{1\text{TeV}} \times 10^{-4} \text{ eV}, \quad (22)$$

and thus small neutrino masses consistent with neutrino flavour oscillation experiments can be obtained.

In summary, active neutrinos in the SM are Weyl particles of left-handed helicity. Due to gauge invariance, they have no bare mass term. However, left-handed neutrinos on the brane couple to the bulk right-handed fermions, and their interaction allows them to acquire a mass. The left-handed bulk fermions do not couple to particles on the brane since their wave function vanishes at $y = 0$, and thus they decouple from the theory.

3.1. Neutrino Mass

Next we examine the mass eigenvalues and eigenstates. For each neutrino flavour, the mass matrix in KK space can be diagonalised independently. Many authors have diagonalised the mass matrix and written down the neutrino mass eigenstates in a variety of different basis. We follow the approach of Cao, Gopalakrishna and Yuan.²⁷

By collecting the neutrino mass terms in the Lagrangian and explicitly including the neutrino flavour indices α and β , we obtain

$$\mathcal{L}_{\text{mass}} = - \sum_{\alpha=1}^3 \sum_{\hat{n}=1}^{\infty} \frac{|\hat{n}|}{R} \psi_R^{\alpha(\hat{n})\dagger} \psi_L^{\alpha(\hat{n})} - \sum_{\alpha,\beta=1}^3 \frac{m_D^{\alpha\beta}}{v} H \left(\psi_R^{\alpha(0)\dagger} + \sqrt{2} \sum_{\hat{n}=1}^{\infty} \psi_R^{\alpha(\hat{n})\dagger} \right) \nu_L^\beta + H.c. \quad (23)$$

We make the Yukawa coupling diagonal in the flavour space by applying the rotations²²

$$\begin{aligned} \nu_L^\alpha &= l^{\alpha i} \nu_L^{\prime i}, & \nu_R^\alpha &= (r^{\alpha i})^* \psi_R^{\prime i(0)}, \\ \psi_L^{\alpha(\hat{n})} &= r^{\alpha i} \psi_L^{\prime i(\hat{n})}, & \psi_R^{\alpha(\hat{n})} &= (r^{\alpha i})^* \psi_R^{\prime i(\hat{n})}, \\ \ell_L^\alpha &= l_\ell^{\alpha i} \ell_L^{\prime i}, & \ell_R^\alpha &= (r_\ell^{\alpha i})^* \ell_R^{\prime i}, \end{aligned} \quad (24)$$

10 *Douglas M. Gingrich*

where the 3×3 unitary matrices l and r are chosen to diagonalise $m_D^{\alpha\beta}$, such that $(r^{\alpha i})^* m_D^{\alpha\beta} l^{\beta j} = m_D^i \delta^{ij}$. The unitary matrices l_ℓ and r_ℓ are similarly chosen to diagonalise the charged lepton mass matrix. This choice of matrices has an advantage in that it does not affect the diagonality of the first term in Eq. (23). The charged current interactions now become proportional to the PMNS matrix^{28–30}

$$V_{\text{PMNS}} \equiv l_\ell^\dagger l. \quad (25)$$

The Dirac spinors can be define via

$$\nu \equiv \begin{pmatrix} \nu_L \\ \psi_R^{(0)} \end{pmatrix}, \nu^{(1)} \equiv \begin{pmatrix} \psi_L^{(1)} \\ \psi_R^{(1)} \end{pmatrix}, \dots, \nu^{(\hat{n})} \equiv \begin{pmatrix} \psi_L^{(\hat{n})} \\ \psi_R^{(\hat{n})} \end{pmatrix}, \dots \quad (26)$$

Also, for each neutrino flavour, the neutrino mass term in the Lagrangian density can be written as

$$\mathcal{L}_{\text{mass}} = \bar{\nu}_D M \nu_D, \quad (27)$$

where $\nu_D^T = (\nu, \nu^{(1)}, \dots, \nu^{(\hat{n})}, \dots)$. In this basis, the mass matrix is

$$M = \begin{pmatrix} m_D & \sqrt{2}m_D P_R \cdots & \sqrt{2}m_D P_R \cdots \\ \sqrt{2}m_D P_L & 1/R & \cdots & 0 & \cdots \\ \vdots & \vdots & \ddots & \vdots & \cdots \\ \sqrt{2}m_D P_L & 0 & \cdots & |\hat{n}|/R & \cdots \\ \vdots & \vdots & \vdots & \vdots & \ddots \end{pmatrix}, \quad (28)$$

where $P_{L/R} \equiv (1 \mp \gamma_5)/2$ are the usual chiral projection operators. This mass matrix is infinite dimensional. The mode number $|\hat{n}|$ is degenerate with degeneracy d_n , and the $|\hat{n}|/R$ elements in the mass matrix are $d_n \times d_n$ block diagonal.

The mass matrix can be diagonalized by two unitary matrices such that $\nu_D = (LP_L + RP_R)\tilde{\nu}_D$, where $\tilde{\nu}_D$ is the mass eigenvector. We can reintroduce the generation index i and the KK index n to write the flavour state ν_L^α in terms of the mass eigenstates $\tilde{\nu}_L^{i(n)}$ as

$$\nu_L^\alpha = l^{\alpha i} L_i^{0n} \tilde{\nu}_L^{i(n)}, \quad (29)$$

where L_i^{0n} is the first row of the L_i unitary matrix.

If we treat the off-diagonal terms in the mass matrix as perturbations^b, then the zeroth-order lightest eigenvalue of the mass matrix is m_D . In the limit

^bThe strong coupling limit has also been investigated.²⁴

$$(m_D R)^2 \sum_{\hat{n}} \frac{d_n}{|\hat{n}|^2} \ll 1, \quad (30)$$

we have, to a good approximation, a Dirac fermion ν with mass m_D , and additional Dirac fermions $\nu^{(\hat{n})}$ with masses $|\hat{n}|/R$. If the neutrino's mass is less than $1/R$, the massive KK modes will have little effect on the neutrino mass term and only the zero mode KK state will generate neutrino mass. In higher order, the lowest mass eigenstate gets an admixture of masses from the KK modes $\psi_R^{(\hat{n})}$. (Note that only the right-handed components of the KK states mix with the SM neutrino). The perturbative limit in Eq. (30) is satisfied when the brane to bulk coupling m_D is small compared to the compactification scale $1/R$. It is also necessary to satisfy Eq. (30) so that the probability of active neutrinos oscillating into the sterile KK states is small.

Adding the second order correction to the lowest mass eigenvalue m_D gives

$$m_\nu = m_D \left[1 - (m_D R)^2 \sum_{\hat{n}} \frac{d_n}{|\hat{n}|^2} \right], \quad (31)$$

where we identify m_ν as the physical SM neutrino mass. For convenience, we define $m_\nu = m_D/N$ and proceed to calculate the correction N^c . This is also the normalisation of the wave function of the lowest eigenstate of the mass matrix. For a single extra dimension, $\hat{n} = n_1 = n$ and there is no degeneracy in the mass matrix ($d_n = 1$). For $\delta > 1$, the states with mass $|\hat{n}|/R$ can be degenerate with degeneracy d_n at the \hat{n} th level. For a large number of KK modes (also possible large $|\hat{n}|$), we can replace the sum over modes by an integral. The leading behaviour is given by the surface of a $(\delta - 1)$ -sphere of radius $|\hat{n}|$ in number space.²⁷ Hence,

$$d_n \approx S_{\delta-1} |\hat{n}|^{\delta-1}, \quad (32)$$

where $S_{\delta-1} = 2\pi^{\delta/2}/\Gamma(\delta/2)$ and Γ is the usual Euler gamma function. In calculations, we sum the number of KK modes up to some maximum. In this case, the heaviest KK state that could be produced is limited by M_D . We denote N_{cut} to be the radius of the biggest sphere in number space such that $N_{\text{cut}}/R = M_D$. The sum over KK states can be divergent and depends on N_{cut} . One can show (see Appendix A) that

$$N^2 = 1 + \left(\frac{m_D}{M_D}\right)^2 \left(\frac{\bar{M}_{\text{Pl}}}{M_D}\right)^2 \times \begin{cases} \frac{\pi^2}{6} \left(\frac{\bar{M}_{\text{Pl}}}{M_D}\right)^2 & \text{for } \delta = 1, \\ 2\pi \ln \left(\frac{\bar{M}_{\text{Pl}}}{M_D}\right) & \text{for } \delta = 2, \\ \frac{2\pi^{\delta/2}}{\Gamma(\delta/2)} \frac{1}{\delta-2} & \text{for } \delta > 2. \end{cases} \quad (33)$$

^cSome authors have defined the same normalisation as \sqrt{N} .

The sum over KK modes converges for $\delta = 1$, is logarithmic divergent for $\delta = 2$, and is power divergent for $\delta > 2$.

The correction N causes the physical neutrino mass to be bounded from above. The upper bound depends on the characteristics of the higher-dimensional space: M_D and δ . The physical mass m_ν does not have an extrema (besides 0) but asymptotically approaches the maximum value

$$m_\nu^{\max} \approx \frac{M_D^2}{M_{\text{Pl}}} \times \begin{cases} \frac{\sqrt{6}}{\pi} \frac{M_D}{M_{\text{Pl}}} & \text{for } \delta = 1, \\ \frac{M_D^2}{\sqrt{2\pi \ln\left(\frac{M_{\text{Pl}}}{M_D}\right)}} & \text{for } \delta = 2, \\ \sqrt{\frac{\Gamma(\delta/2)(\delta-2)}{2\pi^{\delta/2}}} & \text{for } \delta > 2, \end{cases} \quad (34)$$

when $m_D \rightarrow \infty$. However, values of m_D that are too high violate Eq. (30). The mixing between the lightest neutrino of mass m_D and heavier neutrinos introduces a correction to the physical neutrino mass m_ν ,

$$m_\nu \approx \frac{m_D}{\sqrt{1 + \left(\frac{m_D}{m_\nu^{\max}}\right)^2}}. \quad (35)$$

Since there is some uncertainty in where exactly the divergence (for $\delta > 1$) in the sum over KK modes should be cut off, m_ν^{\max} , and thus m_ν , is a bit uncertain. However, m_ν must satisfy $m_\nu < m_\nu^{\max} < m_D$. Only a rigorously formulated theory, such as string theory, could give precise knowledge of the cut-off parameter.

The perturbative condition places constraints on m_D , δ , and R (and M_D due to the cut-off in the summation). Using Eq. (5) we can re-express the condition on R in terms of M_D . Since m_D is not physical, we can replace it by a function of m_ν by using Eq. (35) or replace it by a function of g by use Eq. (21). We discuss the former case next, and then the later case in section 3.3. For one extra dimension and $M_D \sim 1$ TeV, the neutrino mass must be less than about 10^{-19} eV. In the same scenario, to obtain a neutrino mass of 1 eV, $M_D \gtrsim 1000$ TeV. We find this small neutrino mass or large fundamental Planck scale to be unnatural and do not consider one extra dimension. For $\delta > 1$, satisfying Eq. (30) gives the results shown in Fig. 2. Current lower limits on the fundamental Planck scale are consistent with current upper limits on the neutrino mass for $\delta > 1$. For two extra dimensions, rather large values for the fundamental Planck scale and low values for the neutrino mass are required to satisfy the perturbative condition. This makes $\delta = 2$ an unlikely choice in this model. A value of the maximum neutrino mass given by the current limits on atmospheric mixing data of about 0.05 eV would require the fundamental Planck scale to be above about 20 TeV, for $\delta > 2$. In section 3.4, we will discuss a slight modification of the model which relaxes these constraints.

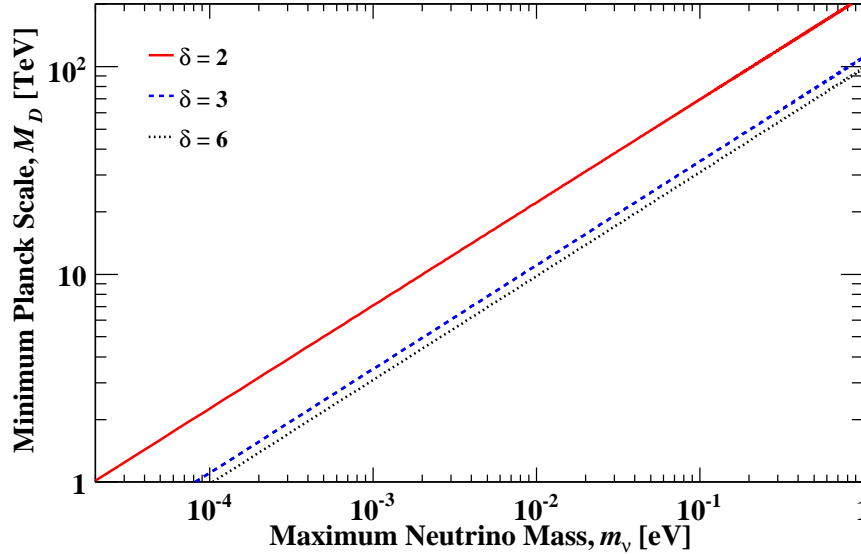


Fig. 2. Minimum fundamental Planck scale M_D versus maximum neutrino mass m_ν required by the perturbative expansion of the mass matrix for two, three, and six extra dimensions.

3.2. Neutrino Mixing

We now briefly consider the implications of higher dimensions on neutrino oscillations. The flavour eigenstates are a non-trivial combination of the physical propagating energy eigenstates that cause the flavour eigenstates to oscillate as a function of time. Good fits to the data from oscillation experiments are obtained by considering only three active species of neutrinos. Strong constraints exist on the mixing of an active neutrino species to a sterile neutrino species.

Let $P_{\nu_\alpha \rightarrow \nu_\beta}$ be the probability of an active neutrino species α oscillating into another active neutrino species β after travelling a distance L . The state of the neutrino after a time t is determined by the Hamiltonian H , and given by the time evolution operator e^{-iHt} . Thus

$$P_{\nu_\alpha \rightarrow \nu_\beta} = \left| \langle \nu_L^\beta | e^{-iHt} | \nu_L^\alpha \rangle \right|^2. \quad (36)$$

Using Eq. (29) and allowing the Hamiltonian to act on the energy eigenstate gives

$$P_{\nu_\alpha \rightarrow \nu_\beta} = \left| l^{\beta i*} l^{\alpha i} |L_i^{0n}|^2 d_n e^{-iE_i^{(n)}L} \right|^2, \quad (37)$$

where $E_i^{(n)}$ is the energy eigenvalue of the n th KK mode of the i th species.

For a neutrino beam with energy E_ν and momentum p_ν , $E_i^{(n)} \approx p_\nu + (m_i^{(n)})^2 / (2E_\nu)$ in the relativistic limit and $m_i^{(n)}$ are the mass eigenvalues. Hence

$$P_{\nu_\alpha \rightarrow \nu_\beta} = \left| l^{\beta i*} l^{\alpha i} \left(|L_i^{00}|^2 e^{-i(L/2E_\nu)m_i^2} + |L_i^{0\hat{n}}|^2 d_n e^{-i(L/2E_\nu)(m_i^{(\hat{n})})^2} \right) \right|^2. \quad (38)$$

The elements of the unitary matrix L_i were given in Ref. 27. Substituting these matrix elements into Eq. (38), summing over β , and assuming $m_{Di}R/\hat{n} \ll 1$ gives

$$\sum_\beta P_{\nu_\alpha \rightarrow \nu_\beta} = 1 - 8 |l^{\alpha i}|^2 \xi_i^2 \sum_{\hat{n}} \frac{d_{\hat{n}}}{\hat{n}^2} \sin^2 \left(\frac{L\hat{n}^2}{4E_\nu R^2} \right) \quad (39)$$

to second order in $m_{Di}R$. We see that the oscillations consists of the interference of an infinite number of modes with increasing frequency $\propto \hat{n}^2$ and decreasing amplitudes $\propto 1/\hat{n}^2$. In practice, the high frequency modes can be averaged and only a few low frequency oscillations can be observed, depending on the energy resolution of the detector.

The probability for an active neutrino state to oscillate into sterile neutrino states ν_s is

$$P_{\nu_\alpha \rightarrow \nu_s} = 1 - \sum_\beta P_{\nu_\alpha \rightarrow \nu_\beta} = 8 |l^{\alpha i}|^2 \xi_i^2 \sum_{\hat{n}} \frac{d_{\hat{n}}}{\hat{n}^2} \sin^2 \left(\frac{L\hat{n}^2}{4E_\nu R^2} \right). \quad (40)$$

We can use the CHOOZ³¹ and atmospheric neutrino data along with Eq. (40) to set bounds on $1/R$. The mass values given in section 2 can be used for each mass hierarchy scheme. We work in a basis in which the charged lepton mass matrix is diagonal. In this case $V_{\text{PMNS}} = l$. For simplicity, we take $\theta_{13} = 0$ and the mixing for atmospheric neutrinos to be maximal with $\theta_{23} = \pi/4$. These simplifications give

$$l = \begin{pmatrix} c_{12} & s_{12} & 0 \\ -s_{12}/\sqrt{2} & c_{12}/\sqrt{2} & 1/\sqrt{2} \\ s_{12}/\sqrt{2} & -c_{12}/\sqrt{2} & 1/\sqrt{2} \end{pmatrix} = \begin{pmatrix} 0.829 & 0.559 & 0 \\ -0.396 & 0.586 & 0.707 \\ 0.396 & -0.586 & 0.707 \end{pmatrix}. \quad (41)$$

The resulting limits²⁷ are given in Table 1. For $\delta > 3$, the active state would oscillate mostly to the heaviest states and we are not able to reliably estimate the oscillation probability. We take these constrains into consideration throughout this paper.

3.3. Neutrino Coupling

Now consider the Higgs interaction term in the action of Eq. (20). The right-handed neutrino does not carry any electroweak quantum numbers and therefore can be produced only through Yukawa interactions. The Higgs boson couples to a tower of KK neutrino states with the same Yukawa coupling ($\sim m_D/v$). In general, the production cross sections and decay widths will be suppressed by the small Yukawa

coupling (since the neutrino mass is small), but enhanced by the sum over a large number ($\sim 10^{30/\delta}$) of KK excitations of bulk fermions.

As mentioned in the previous section, the perturbative condition Eq. (30) can also be expressed in terms of M_D , δ , and g . Equation (21) can be substituted into Eq. (30), and a condition on M_D and g can be obtained for a given δ . For $\delta = 1$, M_D is required to be close to the GUT scale of $\mathcal{O}(10^{16})$ GeV or g is required to be infinitesimally small. Thus a single extra dimension is not of interest to us. For $\delta = 2$, $M_D/g \gtrsim 1$ TeV, and for $\delta > 2$, $M_D/g \gtrsim v$. Both of these conditions should always be satisfied. Thus $M_D \gtrsim 1$ TeV and $g \lesssim 1$ will satisfy the perturbative constraint for all $\delta > 1$. Some cases for specific values δ are shown in Fig. 3.

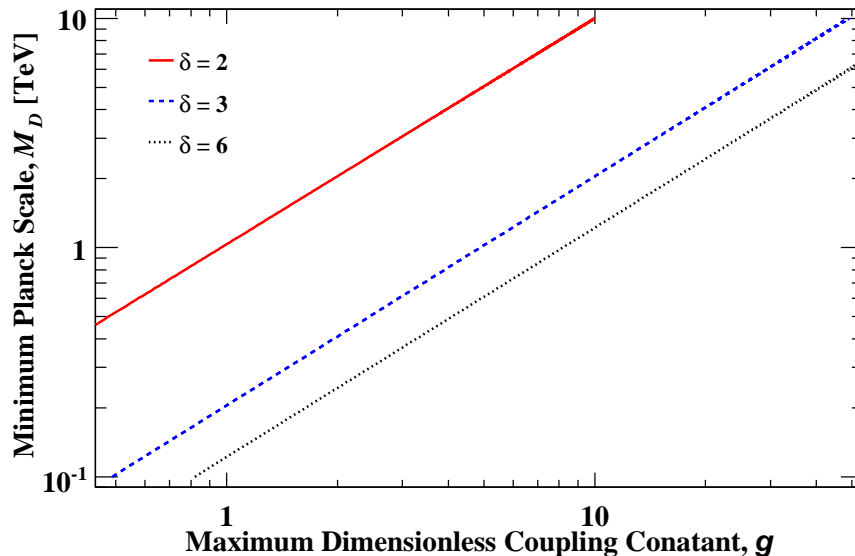


Fig. 3. Minimum fundamental Planck scale M_D versus maximum dimensionless coupling constant g required by the perturbative expansion of the mass matrix for two, three, and six extra dimensions.

Equations (21), (34), and (35) allow us to relate g to the physical neutrino mass m_ν , M_D , and δ . Based on the existing atmospheric neutrino mass best fit of $m_\nu = 0.05$ eV, Fig. 4 shows a plot of the dimensionless coupling constant versus fundamental Planck scale. For a perturbative effective theory, g can not be arbitrarily large.³² For $g \sim 1$, M_D must be about 2000 TeV. This condition has very little dependence on the number of dimensions. If we restrict $g < 10$, the fundamental Planck scale is required to be $M_D > 200 - 300$ TeV. Since the UV cut-off scale for the KK sum is somewhat uncertain, $g \sim \mathcal{O}(10)$ is not an unreasonable possibility, but will violate the perturbative constraint for low M_D . Thus, for the model of large

extra dimensions that we have just considered, M_D is required to be quite large. Hence we consider small modifications to the model in the next subsection.

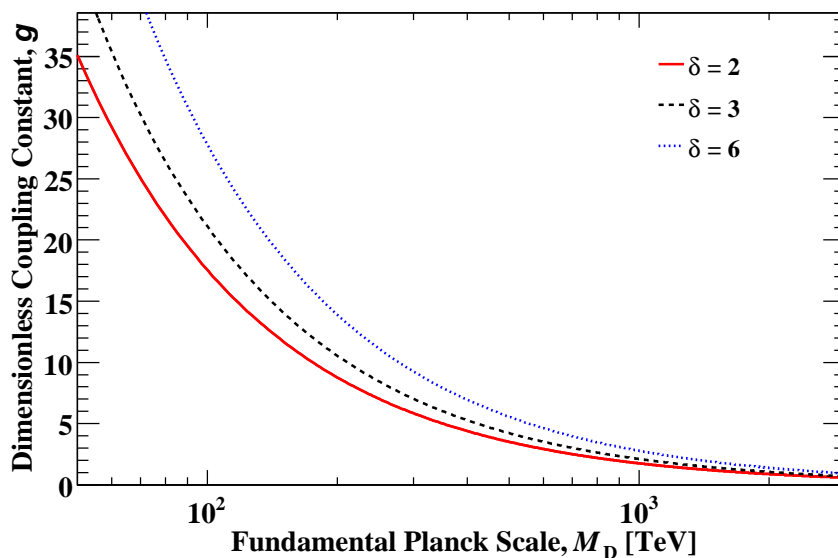


Fig. 4. Dimensionless coupling constant g versus fundamental Planck scale M_D for neutrino mass $m_\nu = 0.05$ eV and 2, 3, and 6 extra dimensions.

3.4. Bulk Fermions in Subspaces and Compactification

A bulk fermion may not necessarily propagate in the same δ extra-dimensional space that the graviton propagates in. It is possible that the bulk fermion propagates in a subset δ_ν of the δ -extra dimensions ($\delta > \delta_\nu$). In fact, different bulk fermions could propagate in different dimensions or the UV cut-off scale could be different for each. Thus the formalism for generating small Dirac neutrino masses that we have discussed so far is merely the specific case of $\delta = \delta_\nu$. Assuming all the extra dimensions are the same size, the necessary substitutions in the above formula are

$$\delta \rightarrow \delta_\nu \quad \text{followed by} \quad \frac{\bar{M}_{Pl}}{M_D} \rightarrow \left(\frac{\bar{M}_{Pl}}{M_D} \right)^{\delta_\nu/\delta}. \quad (42)$$

The generalisation of Eq. (33) is given in Appendix A. In this model, the maximum value of the physical neutrino mass Eq. (34) is given by

$$m_\nu^{\max} \approx M_D \left(\frac{M_D}{\bar{M}_{Pl}} \right)^{\delta_\nu/\delta} \sqrt{\frac{\Gamma(\delta_\nu/2)(\delta_\nu - 2)}{2\pi^{\delta_\nu/2}}} \quad (43)$$

for the case of $\delta > 2$. This is larger than the $\delta_\nu = \delta$ case. The $\delta = 1$ and 2 cases follow trivially.

Although $\delta = 1$ is ruled out in the cases of gravity and in the model just presented, $\delta_\nu = 1$ is not experimentally constrained. However, for bulk fermions in one dimension, $m_D R \ll 1$ will not be satisfied. Figure 5 shows some cases for a bulk fermion living in a subspace of gravity. $M_D \sim \mathcal{O}(1)$ TeV is now possible for $g \sim \mathcal{O}(1)$.

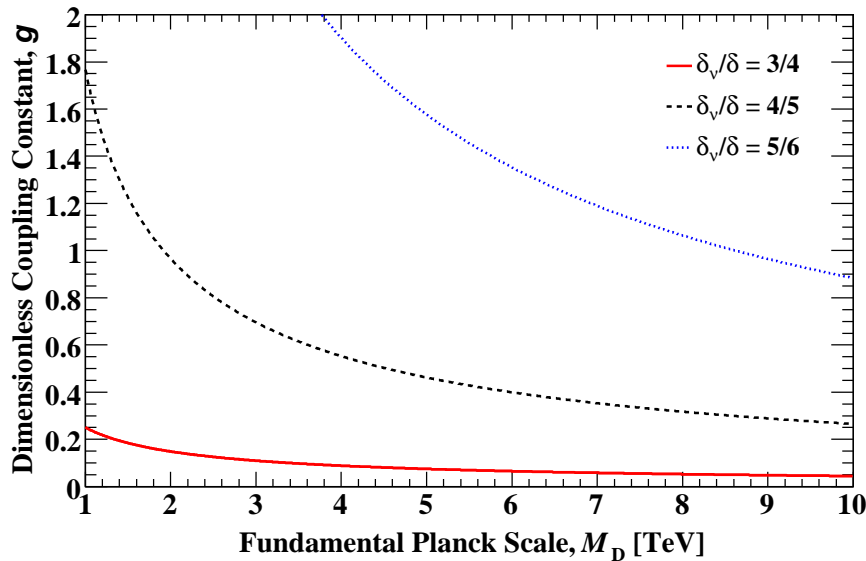


Fig. 5. Dimensionless coupling constant g versus fundamental Planck scale M_D for three different neutrino subspaces of gravity space.

There is no reason for the internal δ -dimensional manifold to be symmetric. One could imagine compactifying on a product of different dimensional tori $\mathcal{T}^\delta = \mathcal{S}^1 \times \mathcal{S}^1 \times \dots \times \mathcal{S}^1$, each with its own characteristic radius R_i . The compactification volume would then be $V_\delta = (2\pi)^\delta R_1 R_2 \dots R_\delta$, and the mass of the KK states would be

$$\sqrt{\sum_i \frac{n_i^2}{R_i^2}}. \quad (44)$$

We can create a simplified version of this scenario by adding three assumptions to the theory. These assumptions are that the bulk fermions propagate in a sub-dimensional space of extra dimensions δ_ν , with common size R , that gravity propagates in the space of extra dimensions δ , and that the extra dimensions $(\delta - \delta_\nu)$

have a common size r with $r \ll R$. With these simplifications Eq. (5) becomes

$$\bar{M}_{\text{P}1}^2 \sim \bar{M}_D^{\delta+2} (2\pi)^\delta R^{\delta\nu} r^{(\delta-\delta\nu)}. \quad (45)$$

In this model, the Dirac mass for the SM neutrino Eq. (21) becomes

$$m_{\text{D}} \approx \frac{g}{\sqrt{2}} \frac{1}{\sqrt{(2\pi\bar{M}_D R)^{\delta\nu}}} v. \quad (46)$$

The volume in Eq. (21) is determined by the compactification scheme. The $(\pi R)^{\delta/2}$ factor in the denominator is identical if compactified on a torus (circle) or a \mathcal{Z}_2 orbifold. However, more interesting scenarios result in different volumes. For example, for a \mathcal{Z}_N orbifold the volume becomes $(2\pi R/N)^{\delta/2}$.

By including such minor modifications as subspace or alternative compactification schemes to the model, most constraints on the model can be avoided. Throughout this paper we will use “rectangular” toroidal geometry for compactification and express the results in terms of the fundamental Planck scale by using Eq. (5). A pedantic review of the subject would express all results in terms of the compactification volume and leave it to the reader to choose the compactification scheme.

We briefly point out yet another consideration in compactification. Compactification manifolds are not only described by their volume but also by their shape. For example, a general 2-torus is described by three parameters: R_1 , R_2 , and θ . Here θ is a shift angle that is usually taken to be $\pi/2$ for a “rectangular” torus. The shape parameters of the general 2-torus are R_2/R_1 and θ . The physical significance of the angle θ is that translations along the R_2 direction produce simultaneous translations along the R_1 direction.³³ Both the volume and shape are important to fully describe the geometry of the compactified extra dimensions. It has been shown that the shape of compactification can dramatically modify the KK spectrum regardless of whether the volume is changed or not.^{33–35} Thus, the compactification scheme would not only affect the phenomenology of models but also their interpretation if extra dimensions were to be discovered.

3.5. Constraints on the Size and Number of Extra Dimensions

To end this section, we briefly discuss some constraints on models of bulk neutrinos in large extra dimensions. Since gravitons at low energies effect SM processes only marginally, the existence of bulk neutrinos generally impose tighter constraints than those due to gravitational interactions on the scale M_D . In the following, we discuss only a few of the many constraints on bulk neutrinos that have been studied. We refer the reader to the literature for constraints due to anomalous magnetic moments of leptons;³⁶ nuclear β -decay in nuclei;³⁷ rare charged lepton processes;³⁸ flavour-violating and universality-breaking phenomena involving W and Z bosons, in addition to leptons;³⁹ perturbative unitarity violation in Higgs-Higgs scattering;²⁷ B meson and top quark decays through a virtual charged Higgs boson and lepton

flavour violating decays through a virtual charged Higgs boson;⁴⁰ neutral pion and neutral B meson decays to invisible decay modes;⁴¹ and cosmological data.⁴²

The luminosity from Supernova 1987a gives strong constraints on extra dimensions.^{43,44} The possible energy loss rate from SN1987a into invisible channels such as the energy carried away by a large number of KK states leads to the following restriction on the size of extra dimensions. The maximum radius of any dimension is $1/R > 10$ keV or $R \lesssim 1$ Å. The limit is independent of the number of dimensions. For $\delta_\nu = \delta = 3$, this constraint requires $M_D \gtrsim 20$ TeV.

A constraint can also be obtained from big bang nucleosynthesis by the need to avoid too much energy being dissipated into bulk KK neutrino modes before the time of nucleosynthesis. This leads an unacceptable expansion rate of the universe. For $\delta_\nu = \delta = 2$, it is likely that too many of the heavy KK modes would be thermal during nucleosynthesis.^{16,17,43,45} This would pose a problem for the expansion of the universe.

Intergenerational mass splitting and mixing in large extra dimensions could lead to the violation of lepton universality and flavour changing processes in the charged lepton sector.⁴⁶ The mixing of a left-handed neutrino with heavy KK modes alters the tau branching ratio and the decay widths of the charged pion, muon, and tau. Based on experimental limits on lepton universality and flavour changing transitions, \bar{M}_D is required to be greater than about 10 TeV for most of the interesting range of neutrino mass splitting.⁴⁶

There are also constraints on the radius of the extra dimensions resulting from data obtained by oscillation experiments. The data restrict the probability of an active neutrino state to mix into a large number of sterile KK bulk neutrino states. Ref. 22 and Ref. 27 derive the bounds shown in Table 1. Atmospheric neutrino measurements provide the most stringent bounds in the normal mass hierarchy, while CHOOZ³¹ data provides the most stringent bounds for the inverted and degenerate mass hierarchies. Ref. 22 uses a model with three active brane neutrinos and three bulk neutrinos. In this case, the results are to be interpreted as constraints on the size of the largest of the extra dimensions, regardless of their total number.

Table 1. Lower bounds on $1/R$ (eV) inferred from oscillation experiments for different mass hierarchies. The results in the first row are from Ref. 22 and constrain the largest extra dimension. The results for 1, 2, 3 extra dimensions are from Ref. 27.

Extra Dimensions	Normal	Inverted	Degenerate
NA	0.24	0.60	10.9
1	0.15	0.5	10.6
2	1.5	5.3	100
3	5.6×10^3	1.2×10^4	10^5

Given the above constraints and to avoid problems with standard big bang nucleosynthesis, we require $\delta > 2$ throughout this paper.

4. Collider Signatures

Testing the origin of small neutrino masses at the LHC is a hot and important topic.^{47,48} There are already many papers on how to test a variety of seesaw mechanisms⁴⁹ and look for heavy Majorana⁵⁰ (or Dirac) neutrinos at the LHC.

If right-handed bulk fermions are responsible for the small mass of a neutrino, what are the consequences at the LHC? Higgs boson production and decay could be measurably altered from SM or supersymmetry (SUSY) expectations. Possible couplings are shown in Figs. 6 and 7. We will use the symbol ν_R to represent the set of right-handed KK states, including the right-handed zero mode. Although right-handed bulk neutrinos would couple to all types of Higgs bosons, we restrict our discussion to the SM Higgs boson and a charged doublet of Higgs bosons.

We review the current bounds on the Higgs boson masses.⁵¹ From electroweak fits and a cut-off scale at the 4-dimensional Planck scale, the SM Higgs boson mass is restricted to $130 < m_H < 180$ GeV^d. If new physics appears at a lower mass scale of 1 TeV, the bounds becomes weaker: $50 < m_H < 800$ GeV. Since $m_H > 114.4$ GeV from the LEP experiments, we do not consider SM Higgs boson masses below 100 GeV. The region $160 < m_H < 170$ GeV has also recently been excluded by the Tevatron experiments.⁵² For the charged Higgs boson, $m_{H^+} > 79.3$ GeV is allowed from the LEP experiments and the Tevatron experiments can limit $m_{H^+} > m_t$ for $\tan \beta < 1$ or $\tan \beta > 40$, where m_t is the top quark mass. We will be interested in charged Higgs bosons that can decay to top quarks and thus limit our considerations to charged Higgs boson masses above 170 GeV.

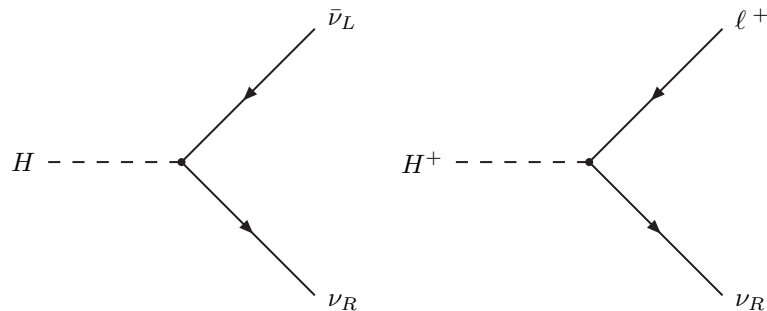


Fig. 6. Higgs boson decays involving right-handed bulk neutrinos.

^dThe neutral Higgs boson will be denoted by H without the neutral charge indicated.

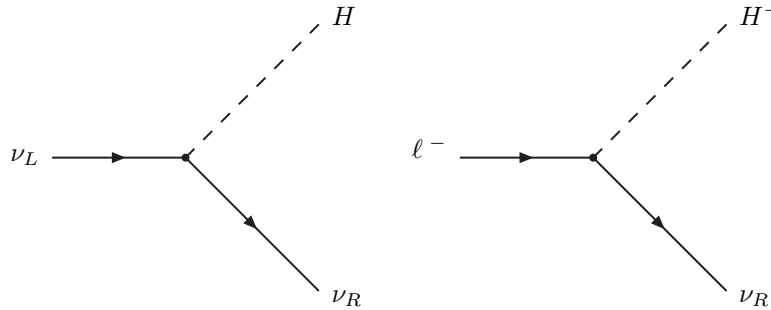


Fig. 7. Higgs boson production involving right-handed bulk neutrinos.

Bulk fermions are not the easiest particles to detect. The KK states behave as massive, noninteracting, stable particles, and thus appear as missing energy in the detector. The ν_L , $\nu_R^{(0)}$, and KK states all lead to missing energy, and their detection must be indirect.

4.1. Tau Decay of a Heavy Charged Higgs Boson

In this section, we review the possibility of a heavy charged Higgs boson decaying to a τ lepton within the model of bulk fermions in large extra dimensions. In typical SUSY models $H^+ \rightarrow \tau_R^+ \nu_L$ is allowed, while $H^+ \rightarrow \tau_L^+ \nu_R$ is completely suppressed^e. Models of bulk fermions in large extra dimensions allow for the possibility of $H^+ \rightarrow \tau_L^+ \nu_R$, where ν_R is a singlet neutrino.

Many extensions to the SM include a charged Higgs boson. We will consider the two-Higgs doublet model of type II (2HDM-II). In this model, each doublet has a unique hypercharge Y . The Higgs doublet with $Y = -1/2$ couples to right-handed up-type quarks and neutrinos, while the Higgs doublet with $Y = +1/2$ couples to right-handed down-type quarks and right-handed charged leptons. An example of such a model is the Minimal Supersymmetric Standard Model (MSSM). In the MSSM there are two vacuum expectation values related by $\tan \beta = v_2/v_1$, where v_2 is the VEV of the $-1/2$ doublet and v_1 is the VEV of the $+1/2$ doublet. The VEV $v = 246$ GeV is given by $v/\sqrt{2} = \sqrt{v_1^2 + v_2^2}$.

In the framework of large extra dimensions with bulk fermions, there is no need to postulate additional Higgs bosons beyond the two doublets. Thus the charged Higgs boson is produced identically as in the 2HDM-II. For a light charged Higgs boson, the dominant production mechanism is through the decay of the top quark $t \rightarrow H^+ b$. To focus the discussion, we consider only a heavy charged Higgs boson

^eIn the following, the charged Higgs boson is denoted by H^+ , but the H^- is also implicitly included.

with mass larger than the top quark mass. We will consider the $2 \rightarrow 2$ production process $g\bar{b} \rightarrow \bar{t}H^+$, as shown in Fig. 8. Charged Higgs boson production in association with a top quark is the dominant process and thus we ignore the processes $b\bar{b} \rightarrow H^+W^-$, $b\bar{b} \rightarrow H^+H^-$, $gg \rightarrow H^+H^-$, and $q\bar{q} \rightarrow H^+H^-$, where q is a light quark.

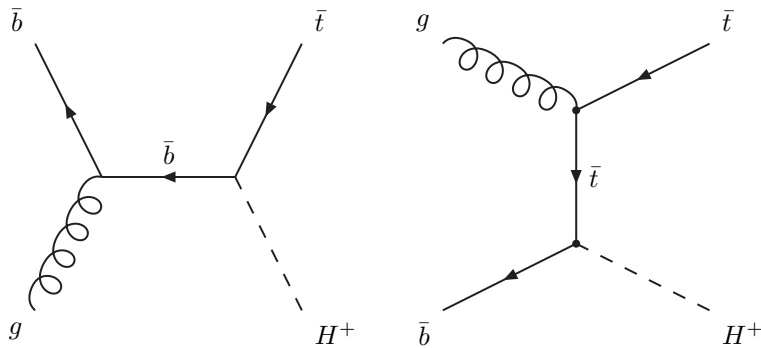


Fig. 8. Leading-order diagrams for heavy charged Higgs boson production in association with a top quark.

Figure 9 shows the leading-order cross section for charged Higgs boson production for masses above the top quark mass. The Yukawa and SUSY electroweak corrections have been calculated along with the one-loop SUSY corrections. The complete next-to-leading order (NLO) QCD corrections have been calculated and are significant. The NLO SUSY-QCD corrections are small in comparison. The next-to-next-to-leading order (NNLO) corrections have been calculated near threshold.^{53–57}

The $2 \rightarrow 3$ process $gg \rightarrow \bar{t}bH^+$ is also possible. This and $g\bar{b} \rightarrow \bar{t}H^+$ overlap when summing the theoretical contributions. Thus one must be careful to avoid double counting when tagging b jets. Alwall and Rathsman⁵⁸ have addressed this problem and provided code⁵⁹ to handle the proper matching in the Monte Carlo generation of events. Double counting has been avoided in Fig. 9 by using Ref. 59.

Branching ratios versus the mass of the charged Higgs boson for two different values of $\tan\beta$ in the MSSM are shown in Fig. 10. The program HDECAY with default parameters has been used.⁶⁰ Above the top quark mass threshold, the $H^+ \rightarrow \bar{t}b$ decay mode dominates. This mode suffers from a large irreducible background and a large combinatorial background. A fraction of heavy charged Higgs bosons are allowed to decay into other modes, depending on the SUSY parameters. Particularly, the decay modes $H^+ \rightarrow \tau^+\nu$ and $H^+ \rightarrow W^+h^0$ can be important. The discovery potential is dominated by $H^+ \rightarrow \tau^+\nu$, which despite its significantly smaller branching ratio for low $\tan\beta$, allows more efficient background suppression. For high charged Higgs boson masses, decays to SUSY particles may be kinemati-

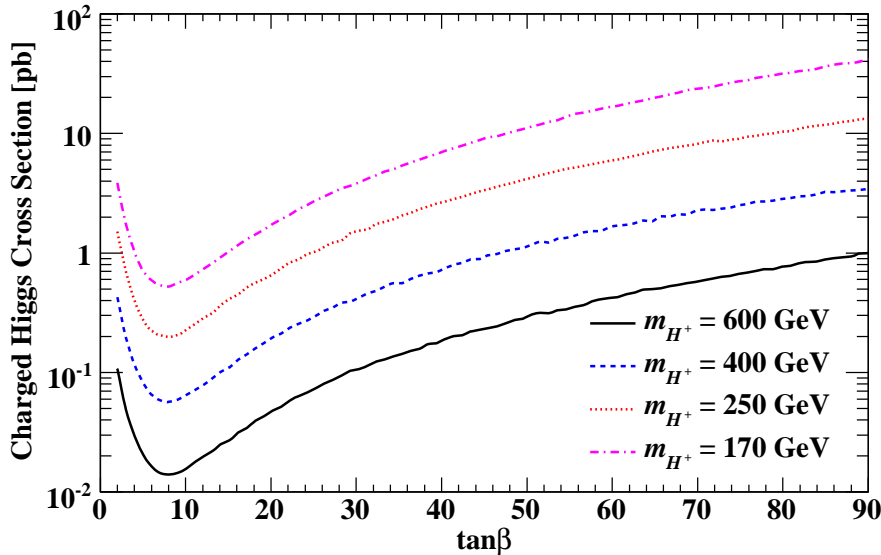


Fig. 9. Leading-order proton-proton cross section at centre of mass energy of 14 TeV for charged Higgs boson production with mass above the top quark mass in the MSSM. The effects of SUSY particles has been ignored.

cally allowed, but we do not consider this possibility. This paper assumes the mass scale of the SUSY partners are above m_{H^+} so that the decays of H^+ to SUSY particles are forbidden.

In the following, we focus on the process

$$g\bar{b} \rightarrow \bar{t}(\rightarrow \bar{b}W^-) H^+(\rightarrow \tau^+\nu). \quad (47)$$

The charged Higgs boson decay to a τ lepton is the strongest one affected by the model of bulk fermions in large extra dimensions.⁴⁰

Although both the W boson and charged Higgs boson can decay to τ leptons, there are important differences in their decays. Unlike the W boson that couples universally to all three leptons, the charged Higgs boson couples preferentially to the heaviest lepton (τ lepton). Since the charged Higgs boson is a scalar particle, the helicities of the final state particles must be different. This is opposite to the decay of the W boson, which is a vector particle. Thus, in the MSSM, $H^+ \rightarrow \tau_R^+\nu_L$ is allowed but $H^+ \rightarrow \tau_L^+\nu_R$ is forbidden (at tree level) since SM neutrinos are left-handed.

For the charged Higgs the corresponding interaction term in the action corresponding to Eq. 20 is

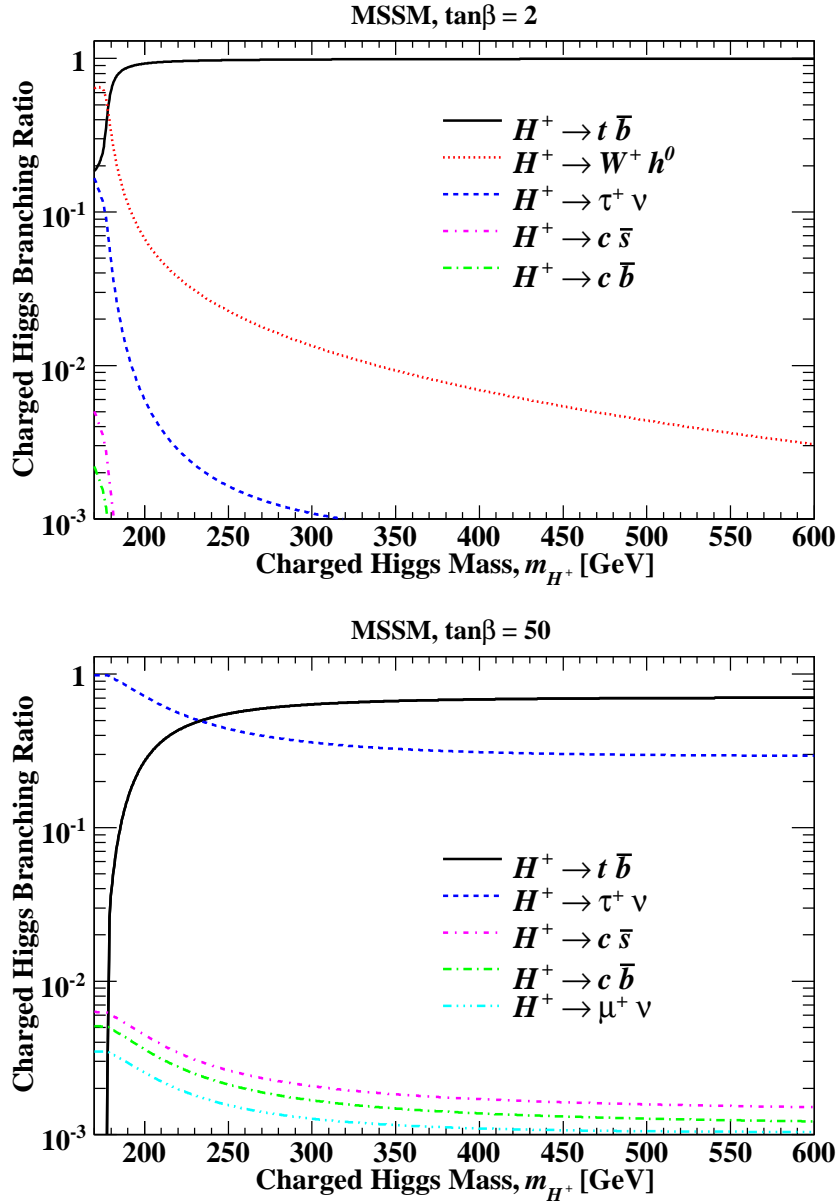


Fig. 10. Branching ratios for charged Higgs boson decays as a function of charge Higgs boson mass in the MSSM for $\tan\beta = 2$ (top) and $\tan\beta = 50$ (bottom). Only decays with branching ratios greater than 0.001 in the charged Higgs boson mass range 170 – 600 GeV are shown.

$$S_{\text{int}} = -\frac{\sqrt{2}}{v} \int d^4x [m_D \cot\beta \bar{\tau}_L H^+ \psi_R + m_\tau \tan\beta \bar{\tau}_R H^+ \nu_L] + H.c. \quad (48)$$

The corresponding couplings are given in Appendix B. Thus, in models of large extra dimensions with bulk fermions, both τ lepton polarizations are allowed: the usual MSSM mode $\tau_R^+ \nu^f$ and the new mode $\tau_L^+ \nu_R$, where ν_R is the right-handed bulk neutrino. The usual charged Higgs boson decays to τ_R leptons through the Yukawa coupling. The SM neutrino ν is now predominantly a light neutrino plus a small admixture of KK modes with mass of order $mR/|\hat{n}|$. Thus this decay is also effected by the presence of the right-handed fermion in the extra dimensions. The decay width $\Gamma(H^+ \rightarrow \tau_R^+ \nu)$ is modified relative to the 2HDM-II calculation, Γ_{MSSM} , provided $m_{H^+} < M_D$ (see Appendix B):⁴⁰

$$\Gamma(H^+ \rightarrow \tau_R^+ \nu) \approx \frac{1+f}{N^2} \Gamma_{\text{MSSM}}(H^+ \rightarrow \tau_R^+ \nu), \quad (49)$$

where

$$f \approx \left(\frac{m}{M_D}\right)^2 \left(\frac{M_{\text{Pl}}}{M_D}\right)^2 \left(\frac{m_H}{M_D}\right)^{\delta-2} x_{\delta-2}, \quad (50)$$

and

$$x_{\delta-2} \approx \frac{2\pi^{\delta/2}}{\Gamma(\delta/2)} \left(\frac{1}{\delta-2} - \frac{2}{\delta} + \frac{1}{\delta+2} \right). \quad (51)$$

In calculating f , the KK states have been summed up to $(m_{H^+} R)^\delta$, i.e. they are required to be lighter than the charged Higgs boson mass (see Appendix C). If $\delta = 2$, $1/(\delta-2)$ must be replaced by $\ln(m_{H^+} M_{\text{Pl}}/M_D^2)$. The quantities in the extra factor $(1+f)/N^2$ partially compensate each other. In the parameter space in which N is large, f will also be large, and when f is small, N is small. The f factor varies with charged Higgs boson mass but over the range 170 to 600 GeV there is little increase in f for low number of extra dimensions. Thus $(1+f)/N^2$ is typically about 0.1 and is always less than unity.

In models of large extra dimensions with bulk fermions, the charged Higgs boson can also decay to a left-handed τ lepton and a right-handed neutrino. A calculation of this decay width gives (see Appendix B)⁴⁰

$$\Gamma(H^+ \rightarrow \tau_L^+ \nu_R) \approx \frac{m_H}{8\pi} \left(\frac{m_D}{v}\right)^2 \cot^2 \beta \left(\frac{m_H}{M_D}\right)^\delta \left(\frac{M_{\text{Pl}}}{M_D}\right)^2 x_\delta, \quad (52)$$

where

$$x_\delta \approx \frac{2\pi^{\delta/2}}{\Gamma(\delta/2)} \left(\frac{1}{\delta} - \frac{2}{\delta+2} + \frac{1}{\delta+4} \right). \quad (53)$$

^fFor the remainder of this subsection, we drop the L subscript on ν_L and consider ν to be either the usual neutrino of the SM or the left-handed neutrino in models of large extra dimensions with bulk fermions.

In the calculation of $\Gamma(H^+ \rightarrow \tau_L^+ \nu_R)$, the τ lepton mass has been neglected and the right-handed neutrino KK states have again been summed up to the threshold for the decays.

In the MSSM at the tree level there are only two parameters: typically chosen to be the mass of the CP-odd scalar Higgs boson m_A and $\tan\beta$. In contrast, the parameter space of a model of large extra dimensions with bulk fermions depends on m_ν , m_{H^+} , $\tan\beta$, M_D , and δ . To get a feel for the relative importance of the two helicity modes, the ratio of decay widths of left-handed to right-handed τ leptons is approximately

$$x_{LR} \sim \frac{\Gamma(H^+ \rightarrow \tau_L^+ \nu_R)}{\Gamma(H^+ \rightarrow \tau_R^+ \nu)} \sim (\cot^4 \beta) \left(\frac{m_D}{m_\tau}\right)^2 \left(\frac{M_{\text{Pl}}}{M_D}\right)^2 \left(\frac{m_{H^+}}{M_D}\right)^\delta, \quad (54)$$

where for simplicity the normalisation due to mixing N^2 , and the phase space factors x_δ and $x_{\delta-2}$ have been ignored. For typical parameter values, $x_{LR} \sim 10^5$. Part of this high value of x_{LR} is because the decay width to τ_R is suppressed by a factor of about 10 relative to the 2HDM-II, as discussed previously. The major factor that results in x_{LR} being high is a large multiplicity factor due to the large number of KK states, despite a small Yukawa coupling to τ_L and a single KK neutrino. The value of x_{LR} can also be low for high M_D and high $\tan\beta$.

Figures 11 and 12 show charged Higgs boson branching ratios for models of large extra dimensions with bulk fermions. Three extra dimensions was chosen and a value of $M_D = 20$ TeV was used to ensure the neutrino masses were consistent with the atmospheric neutrino data. Dirac masses of $m_D = 0.1$ eV (corresponding to $m_\nu^2 = 1.8 \times 10^{-3}$ eV²) and $m_D = 3$ eV (corresponding to $m_\nu^2 = 2.2 \times 10^{-3}$ eV²) have been chosen to lie in the allowed experimental range. For small m_D , we see similar decay branching ratios for models of large extra dimensions with bulk fermions as in the MSSM. As m_D gets larger, $H^+ \rightarrow \tau^+ \nu$ becomes dominant for small $\tan\beta$ values.

In searching for the effects of bulk neutrinos in charged Higgs boson decay, we need to both extract a signal of charged Higgs boson events above background events, and show that the resulting signal events agree with the large extra dimensions scenario. If one tries to just exploit the τ lepton polarization difference to separate bulk fermions in large extra dimension models from the MSSM, one is probably not able to reduce the background from SM W boson decays, as these have the same signature as our extra dimensional model signal. First, we must reduce the SM background to get a clean sample of charged Higgs boson events. After this, an attempt can be made to use the τ lepton polarization to determine the charged Higgs boson decay mechanism, and hence, rule out the MSSM or large extra dimensions model.

One of the backgrounds to our production channel of interest is single top quark production $gb \rightarrow Wt$, where the W boson mimics the charged Higgs boson. The cross section times branching ratio for this background is about 48 pb. Another

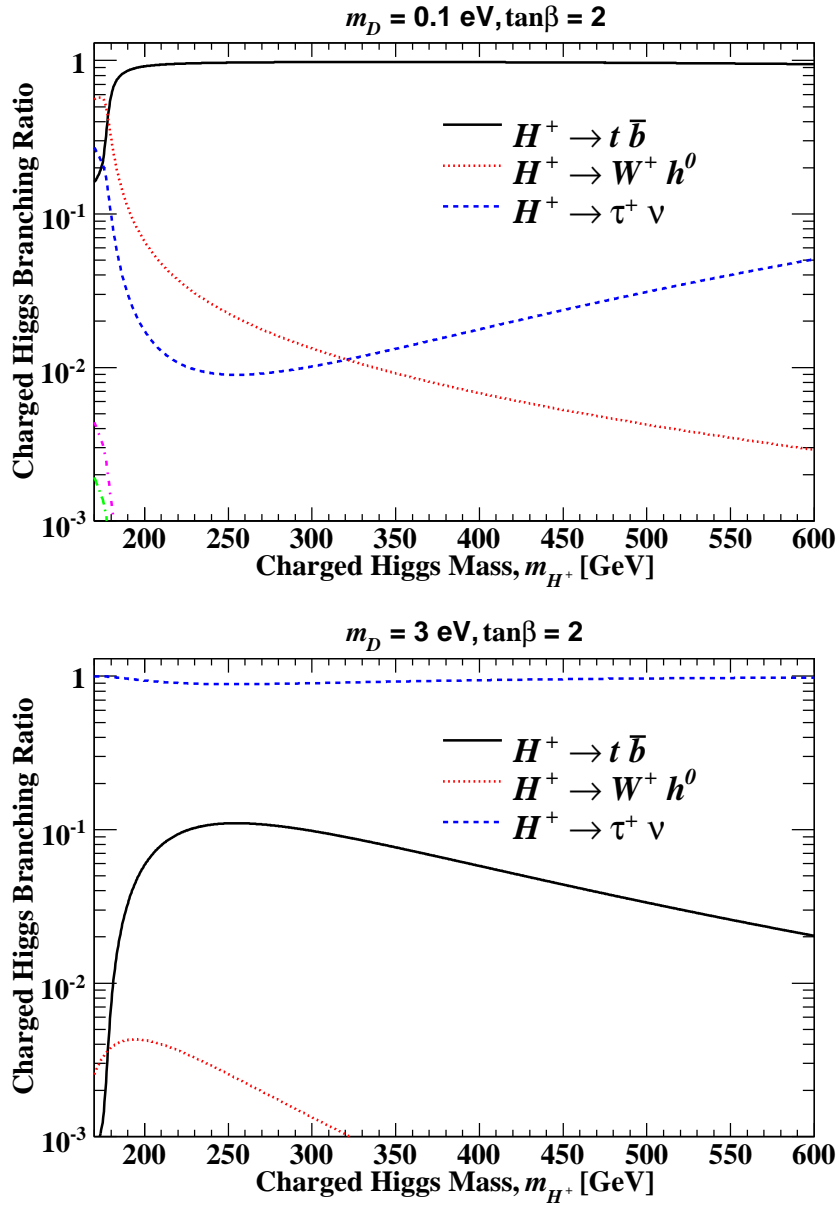


Fig. 11. Branching ratios for charged Higgs boson decays as a function of charge Higgs boson mass for $\tan\beta = 2$, $M_D = 20$ TeV, $\delta = 3$, and $m_D = 0.1$ eV (top) and $m_D = 3$ eV (bottom). Only decays with branching ratios greater than 0.001 in the charged Higgs boson mass range 170 – 600 GeV are shown.

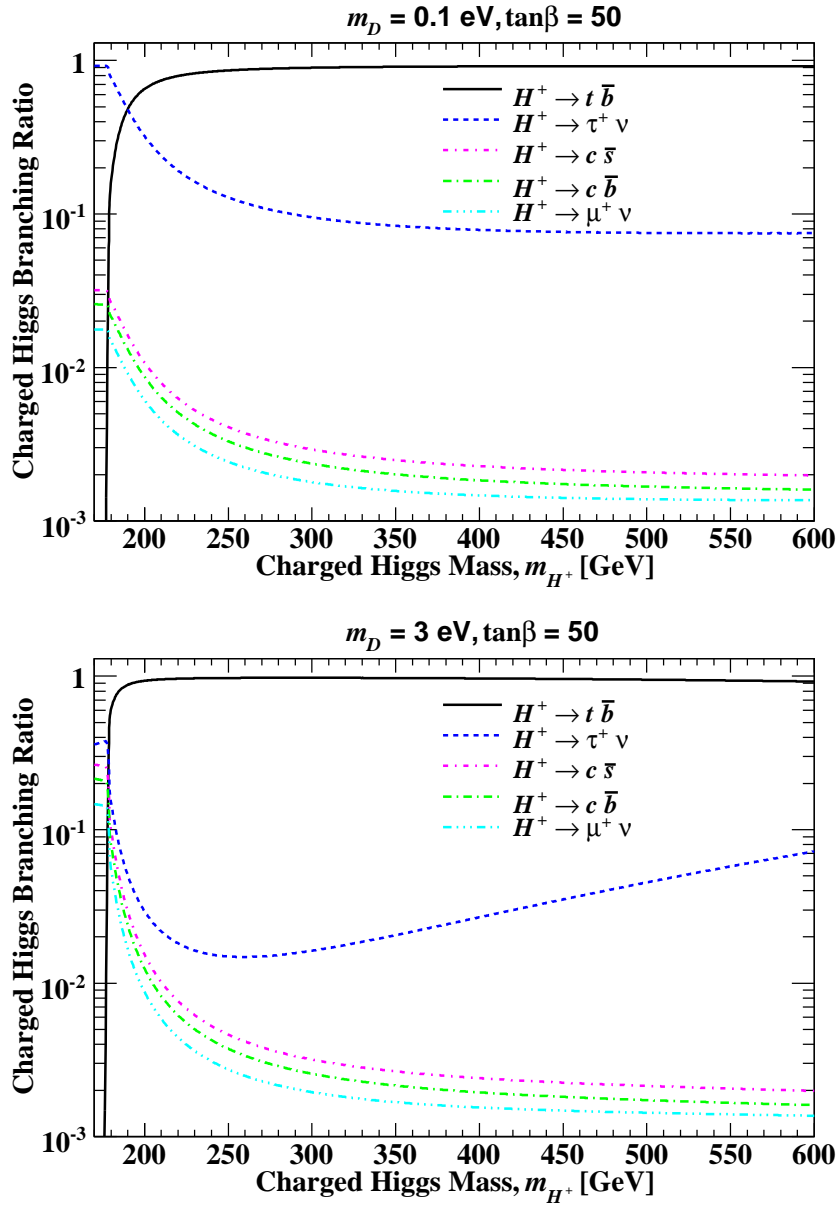


Fig. 12. Branching ratios for charged Higgs boson decays as a function of charge Higgs boson mass for $\tan\beta = 50$, $M_D = 20 \text{ TeV}$, $\delta = 3$, and $m_D = 0.1 \text{ eV}$ (top) and $m_D = 3 \text{ eV}$ (bottom). Only decays with branching ratios greater than 0.001 in the charged Higgs boson mass range 170 – 600 GeV are shown.

background is $t\bar{t}$ production with one $W \rightarrow jj$ and the other $W \rightarrow \tau_L\nu$. The cross section times branching ratio for this background is about 84 pb. For the signal, the cross section times branching ratio can be about 0.04 pb to 3.46 pb over the charged Higgs boson mass range of 200 – 500 GeV and $\tan\beta$ from 1.5 to 30. The background will need to be reduced by a factor of about 40 to 3000. The above branching ratio times cross section values have been obtained from Ref. 61.

The differences between signal and background have been examined in Refs. 61, 62, and more recently, in Ref. 51. We largely follow the discussion in Ref. 61. Since we are interested in the τ lepton decay modes of the charged Higgs boson, we require a well reconstructed τ jet. One-prong hadronic decays of the τ lepton are identified and the reconstructed τ jet is required to have high transverse momentum p_T^τ to reduce the soft τ jet backgrounds. The reason we chose single-prong hadronic τ lepton decays will be explained when we discuss measuring the τ lepton polarization.

Since the charged Higgs boson is produced in association with a top quark, we reconstruct single top quark events. Typically, at least three non- τ jets with high p_T would be required. One of these jets, and only one, would need to be tagged as a b jet. Two of the non-tagged b jets would be required to have an invariant mass close to the W boson mass. These two jets would have their energy adjusted to reproduce the W boson mass and the resulting energy-rescaled jets would be combined with the b jet to reconstruct the three-jet invariant mass. Events with a three-jet invariant mass close to the top quark mass would be selected for further analysis.

The difference in mass between the charged Higgs boson and the W boson can also be exploited. The W bosons are highly boosted in the laboratory frame of reference and hence the τ lepton is approximately collinear with the neutrino along the direction of the original W boson. Thus the distribution of the azimuthal opening angle $\Delta\phi$ between the τ jet and the missing transverse energy[§] \cancel{E}_T should be peaked at small values for W boson decays. The azimuthal angle $\Delta\phi$ should be larger for τ leptons from charged Higgs boson decays.

The difference in mass between the charged Higgs boson and the W boson can be exploited further. Because of the neutrino in the final state, only the transverse mass can be reconstructed:

$$m_T = \sqrt{2p_T^\tau \cancel{E}_T [1 - \cos(\Delta\phi)]}. \quad (55)$$

In background events, the transverse mass has an upper bound at the W boson mass, while in the signal events it is constrained by the charged Higgs boson mass. However, due to finite resolution (particularly on \cancel{E}_T), there is leakage of the background into the signal region. To optimise the signal to background ratio, a requirement is imposed on the transverse mass ($m_T > 100$ GeV, for example). In addition, a cut

[§]Although we call this quantity missing transverse energy, we really mean the negative of the vector sum of all the visible transverse momenta in the event.

on $\Delta\phi$ ($\Delta\phi > 1.0$, for example) can be applied. Using such a set of requirements as described above and a simple simulation of the ATLAS detector, Assamagan and Deandrea⁶¹ have shown that a significance (defined by S/\sqrt{B}) greater than five can be obtained with 100 pb^{-1} of data. Using a detailed simulation of the ATLAS detector, the charged Higgs boson should be detectable in a significant fraction of the $(\tan\beta, m_{H^+})$ parameter space with the first 10 fb^{-1} of data.⁵¹ The discovery reach is most likely limited by the signal size itself.⁶¹

Observation of a signal in the transverse mass and azimuthal opening angle distributions could help one to obtain a clean sample of charged Higgs boson events. Unfortunately, this would not allow one to determine whether the scenario is the MSSM or not. A further measurement of the polarization asymmetry might provide distinctive evidence for models with bulk fermions in large extra dimensions. We can look at the τ lepton polarization asymmetry which is defined as

$$A_\tau = \frac{\Gamma(H^+ \rightarrow \tau_L^+ \nu_R) - \Gamma(H^+ \rightarrow \tau_R^+ \nu)}{\Gamma(H^+ \rightarrow \tau_L^+ \nu_R) + \Gamma(H^+ \rightarrow \tau_R^+ \nu)}. \quad (56)$$

In the 2HDM-II, A_τ is -1 . In the model of bulk fermions in large extra dimensions, $A_\tau \sim -1$ is also allowed but $H^+ \rightarrow \tau_R^+ \nu$ would have a different phase space since the neutrino contains an admixture of KK modes. For small values of m_ν the τ lepton is right-handed (except for small values of $\tan\beta$). Left-handed τ leptons are produced for large m_ν .

To study the τ lepton polarization, consider the hadronic single-prong decays

$$\begin{aligned} \tau^- &\rightarrow \pi^- \nu && (11\%), \\ \tau^- &\rightarrow \rho^- (\rightarrow \pi^- \pi^0) \nu && (25\%), \\ \tau^- &\rightarrow a_1^- (\rightarrow \pi^- \pi^0 \pi^0) \nu && (9\%). \end{aligned} \quad (57)$$

These decays best imprint the information of the τ polarization onto the decay products. Experimentally, one does not distinguish between π and K mesons, and ρ and K^* mesons. Thus a small contribution from the kaon modes is present. The above decays correspond to about 90% of the hadronic one-prong decays and thus should represent the τ lepton polarization effects. We make the approximation that the decay products of the τ lepton merge along the τ lepton line of flight in the laboratory frame (collinear approximation).

To take advantage of the direction of the charged π meson encoding the τ lepton information, the momentum of the π meson p_π relative to the energy of the τ jet E_τ , $x \equiv p_\pi/E_\tau$, could be examined. The ratio x is related to the angle that measures the direction of the charged hadron in the τ lepton rest frame relative to the τ lepton line of flight, which defines its polarization axis.⁶³ In the case of MSSM, the π mesons coming from charged Higgs boson decays are peaked at $x = 1$. The distribution is peaked at $x = 0$ and $x = 1$ for longitudinal ρ and a_1 mesons, but is in the middle for transverse ρ and a_1 mesons. In the case of models with bulk fermions or background due to $W \rightarrow \tau_R \nu$ decay, the contributions to the x distribution are

reversed; the π mesons coming from the W boson decays are peaked at $x = 0$. Since it is anticipated that the discover reach is limited by the signal size itself, the backgrounds, after the above reduction, are expected to be very small. Thus the x distribution could be examined to reveal the model for charged Higgs boson decays. The distribution should be peaked at $x = 0$ and $x = 1$ for the MSSM. For models of bulk fermions in large extra dimensions, the x distribution would depend on the polarization asymmetry. In the case of a polarization asymmetry of about one (about 100% left-handed τ leptons) the x distribution would be peaked near the centre.

In summary, although one could claim a discovery by observing a charged Higgs boson, it would be insufficient to say what beyond the SM physics produced it. Further measurement of the polarization asymmetry might provide distinctive evidence for the model of bulk fermions in large extra dimensions.

4.2. Invisible Decay of a Light Higgs Boson

Higgs boson invisible decays have been discussed in a number of models for physics beyond the SM.⁶⁴ To trigger on the invisible decay mode of the Higgs boson, the Higgs boson must be produced in association with other particles. In addition, one can not reconstruct the Higgs boson directly but must probe the signal indirectly through the missing energy distribution.

For invisible Higgs boson decay in models of bulk neutrinos, no additional production mechanisms beyond the SM are necessary. The cross sections for SM Higgs boson production are shown in Fig. 13. The gluon-gluon fusion channel, via a top quark loop, is dominant. However, since there is nothing else in the event besides the Higgs boson, this channel is of little use for triggering on Higgs boson invisible decays. The vector-boson vector-boson fusion process ($qq \rightarrow qqV^*V^* \rightarrow qqH$) has recently been shown to be a viable channel for triggering and searching for Higgs boson invisible decays.⁵¹ Because of its large cross section, it has become a channel of interest. The jets are preferentially separated in rapidity and are correlated in azimuthal angle. A low-luminosity trigger, which triggers on missing transverse energy plus a forward jet plus a central jet is possible. At higher luminosity there will be more activity in the rapidity gap and it is not known how effective the trigger will be. Further discussion of this channel is beyond the scope of this phenomenological review. Other useful channels are the Higgs-strahlung processes ($q\bar{q}' \rightarrow VH$), or associated production with a vector boson, and associated production with a top quark. Associated production with a top quark has not received much attention and it is anticipated to be less useful than the Higgs-strahlung processes.

Associated production with the W boson occurs via $q\bar{q}' \rightarrow W^* \rightarrow WH$, which is followed by $W \rightarrow \ell\nu$ and $H \rightarrow$ invisible. The composite signature to be observed from this decay is 1) no hadronic activity, 2) missing transverse momentum, and 3) a high- p_T lepton. Background due to off-shell W^* production and its leptonic decay overwhelm the signal channel by a factor of more than 200 even after background

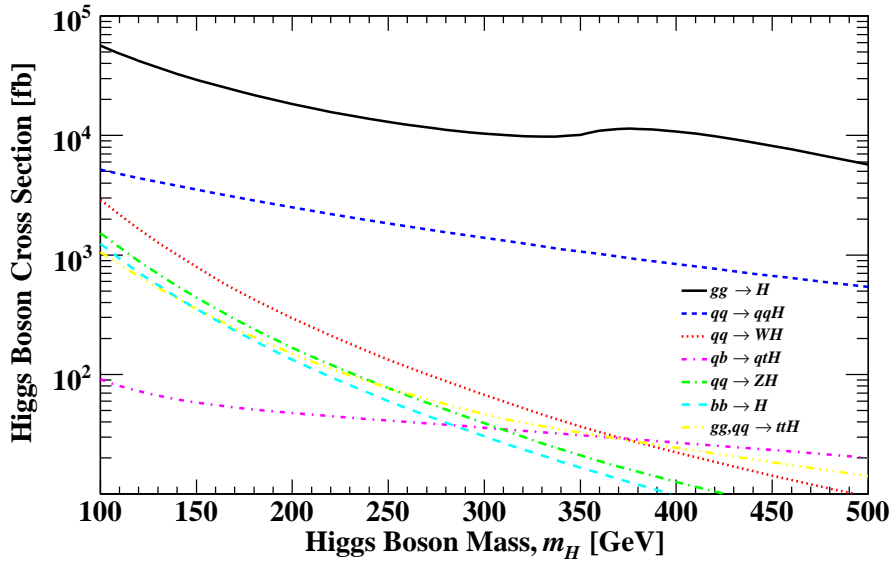


Fig. 13. Proton-proton cross section at a centre of mass energy of 14 TeV for Standard Model Higgs boson production versus Higgs boson mass.

rejection cuts.⁶⁵ We will examine this process in more detail in the next subsection.

A better channel is associated production with the Z boson

$$q\bar{q} \rightarrow Z^* \rightarrow ZH, \quad (58)$$

where $Z \rightarrow \ell^+\ell^-$ ($\ell = e$ or μ only) and $H \rightarrow$ invisible. The τ lepton decay mode of the Z boson is usually not considered because of uncertainties in τ lepton identification and the resulting poor invariant mass resolution from using τ leptons to reconstruct Z bosons. The signature from the decay is 1) no hadronic activity, 2) missing transverse momentum, and 3) two high- p_T same flavour charged leptons with invariant mass close to the mass of the Z boson. The two high- p_T leptons trigger the event.

There is an irreducible background to the process in Eq. (58) from ZZ production, where one Z boson decays leptonically and the other Z boson decays into neutrinos. Since ZZ is produced by t -channel processes, it is expected that the p_T distribution of the Z bosons will be softer than the p_T distribution of the Z bosons from the ZH s -channel production process. The next most significant irreducible background is from WW production with each W decaying leptonically. This background has a considerably softer transverse momentum distribution. Since both of these backgrounds have softer transverse momentum distributions than the signal, to may be possible to detect a signal by requiring high missing transverse energy.

Other backgrounds arise from WZ , Wj , and $Z^* \rightarrow \tau^+\tau^- \rightarrow \ell^+\ell^- + \cancel{E}_T$, but they can be suppressed.

The $Z \rightarrow b\bar{b}$ decay channel must also be considered in the process in Eq. (58). The advantage of this channel is the increased branching fraction of $Z \rightarrow b\bar{b}$ compared to $Z \rightarrow \ell^+\ell^-$. The disadvantages are the lower efficiency for identifying $b\bar{b}$ final states compared to leptonic final states, the reduced Z boson invariant mass resolution, and the more difficult background sources. These backgrounds include contributions from ZZ , WZ , $Zb\bar{b}$, $Wb\bar{b}$, single top quark, and $t\bar{t}$ production. The significance of the $Z \rightarrow b\bar{b}$ channel is not as high as in the lepton channel, but this channel could be combined with the lepton channel, or be used to confirm an observed signal. Another potential background to the process in Eq. (58) is $Z \rightarrow \nu\bar{\nu}$ and $H \rightarrow b\bar{b}$.

The SM Higgs boson can decay to ν_L plus a right-handed bulk neutrino in models of large extra dimensions. The invisible decay width summed over all neutrino flavours is (see Appendix B)^{17,41,64}

$$\sum_{n=0}^{m_H R} \Gamma(H \rightarrow \nu_L \bar{\nu}_R^{(n)}) \sim \sum_{n=0}^{m_H R} \frac{m_H}{4\pi} \left(\frac{m_D}{v}\right)^2 \left(1 - \frac{m_{\nu_R^{(n)}}^2}{m_H^2}\right) d_n \sim \frac{m_H}{16\pi} \left(\frac{m_D}{v}\right)^2 (m_H R)^\delta. \quad (59)$$

The Higgs boson decay to the final state $\nu_L \bar{\nu}_R$ is proportional to $(m_D/v)^2$ which is extremely small. However, the multiplicity of KK states below m_H is $(m_H R)^\delta$, which can be very large. It is proportional to the volume R^δ of the δ -dimensional space times a momentum-space factor of order m_H^δ .

Figure 14 shows the Higgs boson branching ratios versus Higgs boson mass for SM processes and a model with bulk fermions in large extra dimensions. Below a Higgs boson mass of 135 GeV the $H \rightarrow b\bar{b}$ decay mode dominates, while above 150 GeV the decay mode $H \rightarrow WW^*$ dominates.

Since $H \rightarrow b\bar{b}$ dominates at low Higgs boson masses, it is useful to consider the ratio

$$\frac{BR(H \rightarrow \nu_L \bar{\nu}_R)}{BR(H \rightarrow b\bar{b})} = \frac{m_D^2}{3m_b^2} \left(\frac{M_{Pl}}{M_D}\right)^2 \left(\frac{m_H}{M_D}\right)^\delta. \quad (60)$$

Figure 15 shows the ratio in Eq. (60) versus fundamental Planck scale. The invisible decay mode of the Higgs boson is significant for $\delta = 3$ and low M_D . For $M_D > 30$ TeV, the invisible decay width of the Higgs boson will be negligibly small compared to $H \rightarrow b\bar{b}$. One way to reduce M_D is to consider a bulk fermion propagating in a subspace δ_ν of the full extra dimensions δ (see section 3.4). With $\delta_\nu = 5$ and $\delta = 6$, M_D can now be as low as a TeV. Only in a very small region of parameter space can the invisible decay of the Higgs boson be as large as the $H \rightarrow b\bar{b}$ decay mode. The main restriction comes from the perturbative constraint on the Yukawa coupling g . Asymmetric dimensions also allow us to reduce M_D while keeping $g \sim \mathcal{O}(1)$.

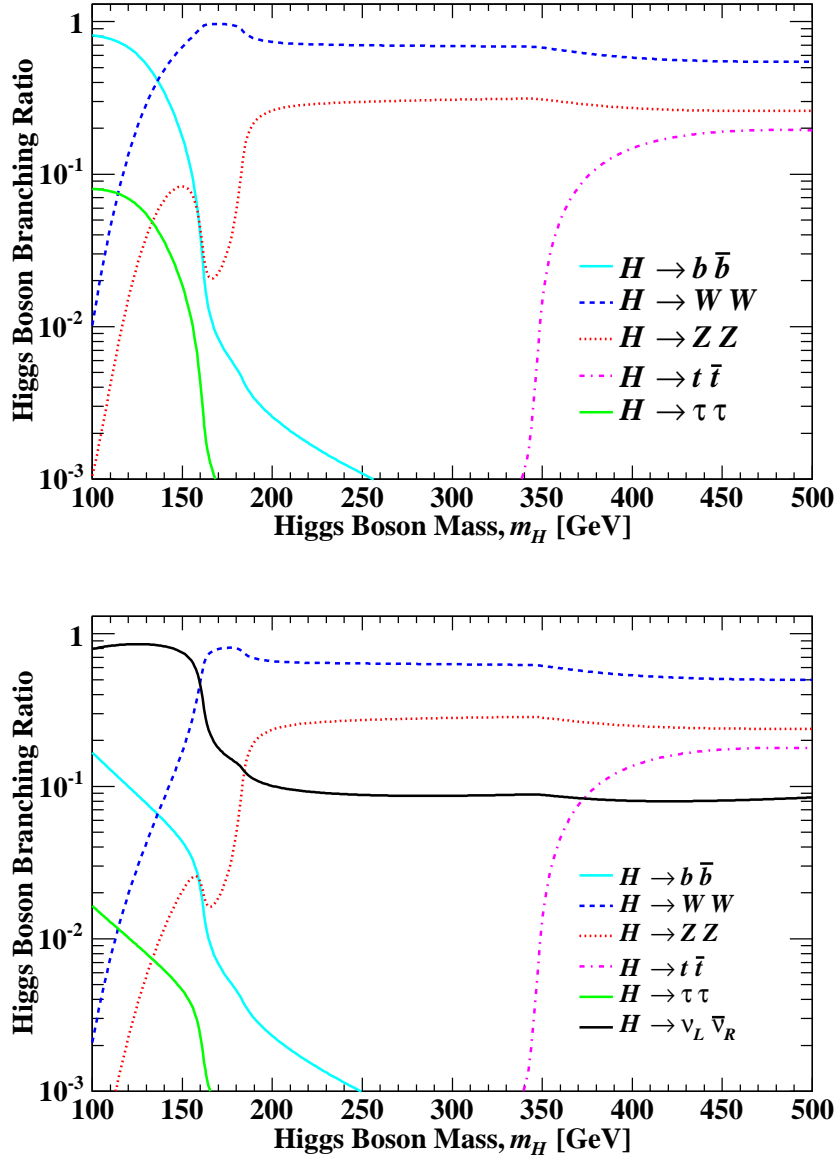


Fig. 14. Branching ratios for Standard Model Higgs boson decays as a function of Higgs boson mass (top) and for a model of bulk fermions in large extra dimensions with $\delta = 3$, $M_D = 22$ TeV, and $m_\nu^2 = 3 \times 10^{-3}$ eV² (bottom). Only decays with branching ratios greater than 0.001 in the Higgs boson mass range 100 – 500 GeV are shown.

Recently, the ATLAS collaboration has performed a detailed study of its detector's sensitivity to an invisibly decaying Higgs boson.⁵¹ Model independent limits

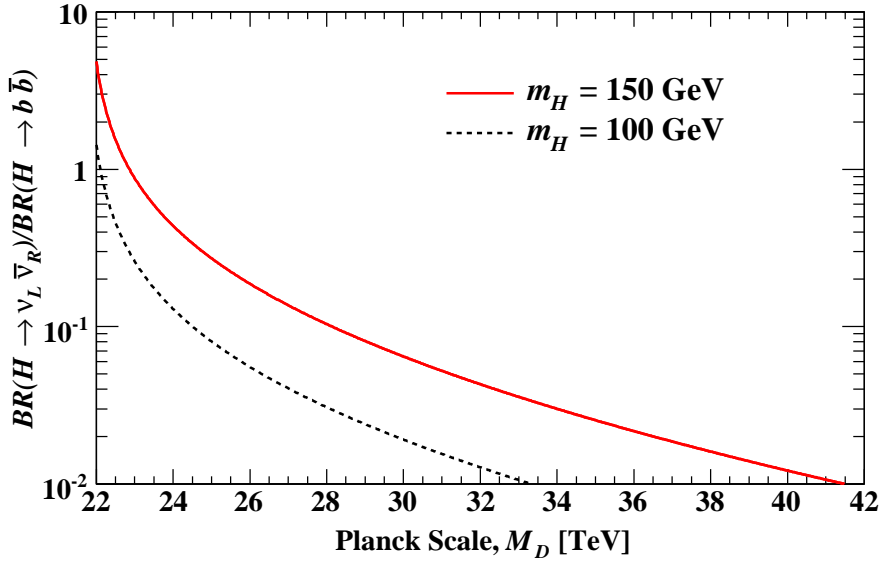


Fig. 15. Ratio of Higgs boson invisible decay width to $b\bar{b}$ decay width versus fundamental Planck scale M_D for two different Higgs boson masses, and $\delta = 3$ and $m_\nu^2 = 3 \times 10^{-3} \text{ eV}^2$.

were set on the branching ratio time cross section divided by the SM Higgs boson cross section. Assuming the SM Higgs boson production cross section for models of bulk fermions, limits can be set on the invisibly decay branching ratio as a function of the neutrino mass, fundamental Planck scale, and the number of extra dimensions. For three extra dimensions and a bulk Dirac fermion mass $m_D = 0.1 \text{ eV}$, lower limits can be set on the fundamental Planck scale. Figure 16 show the derived lower limits on the fundamental Planck scale using the vector boson fusion limits in Ref. 51.

In summary, in certain regions of extra-dimensional parameter space, the branching ratio of Higgs boson decay into invisible modes can be greater than $BR(H \rightarrow b\bar{b})$, but the Yukawa coupling g is large. For reasonable values of g , the invisible decay rate is a tiny fraction of the $H \rightarrow b\bar{b}$ rate.

4.2.1. Associated Production of Bulk Neutrino with Light Higgs Boson

We now discuss in more detail the process of off-shell W^* production and its leptonic decay. Consider the process (Fig. 17)

$$q\bar{q}' \rightarrow W^* \rightarrow \ell^+ H \nu_R, \quad (61)$$

where ν_R is a KK mass eigenstate. The process is mediated by ν_L .

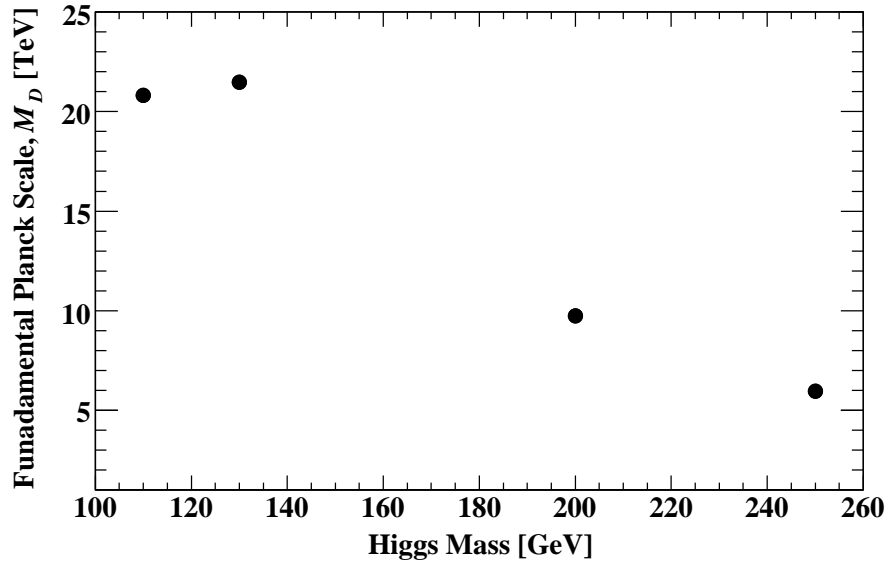


Fig. 16. Derived 95% confidence level lower limits on the fundamental Planck scale M_D versus Higgs boson mass from limits on an invisible decaying Higgs boson from Ref. 51, assuming $\delta = 3$ and $m_D = 0.1$ eV.

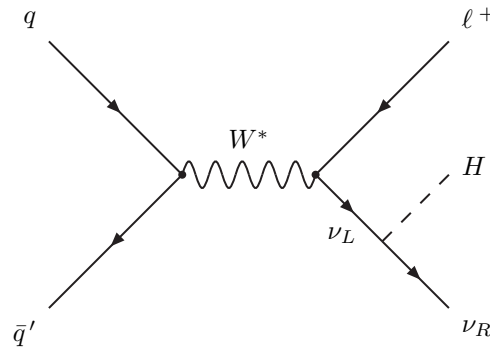


Fig. 17. Associated production of the neutral Higgs boson with a charged lepton.

In calculating the cross section, we again work in a basis in which the charged lepton mass matrix is diagonal and l is given by Eq. (41). Cao, Gopalakrishna, and Yuan⁶⁸ have shown that it is also beneficial to work in a bases in which ψ_R^α is rotated with matrix r , since this absorbs the unphysical matrix r into the definition of ψ'_R . It was also found that one should retain ν_L in the flavour basis in order to explicitly keep only the physical matrix l . In this basis, the total production rate for

process in Eq. (61), summed over all lepton flavours, is proportional to $\sum_{i,\ell} |\bar{m}_D^{i\ell}|^2$, where $\bar{m}_D \equiv m_\nu^d l^\dagger$, and m_ν^d is a 3×3 physical diagonalised neutrino mass matrix. Using the neutrino data in section 2, the matrix \bar{m}_D in each mass hierarchy scheme is

$$\bar{m}_D(\text{normal}) = \begin{pmatrix} 0 & 0 & 0 \\ 0.0050 & 0.0053 & -0.0053 \\ 0 & 0.0354 & 0.0354 \end{pmatrix}, \quad (62)$$

$$\bar{m}_D(\text{inverted}) = \begin{pmatrix} 0.0414 & -0.0198 & 0.0198 \\ 0.0280 & 0.0293 & -0.0293 \\ 0 & 0 & 0 \end{pmatrix}, \quad (63)$$

$$\bar{m}_D(\text{degenerate}) = \begin{pmatrix} 0.829 & -0.396 & 0.396 \\ 0.559 & 0.586 & -0.586 \\ 0 & 0.707 & 0.707 \end{pmatrix}, \quad (64)$$

and the $\sum_{i,\ell} |\bar{m}_D^{i\ell}|^2$ values are $(0.0509 \text{ eV})^2$ for the normal, $(0.0707 \text{ eV})^2$ for the inverted, and $(1.732 \text{ eV})^2$ for the degenerate mass hierarchy schemes.

The cross section summed over all lepton flavours $\ell = e, \mu$, and τ as a function of m_ν , m_H , $1/R$, and δ has been calculated in Ref. 68. The cross section is less than a femtobarn for $\delta = 2$, so we will focus on $\delta = 3$. The cross section decreases slightly with increasing Higgs boson mass. However, the main dependence is on $1/R$ (or M_D) with $\sigma \sim 10^3 - 10^{-3} \text{ fb}$ for $M_D = 2 - 20 \text{ TeV}$. Besides the new physics production mode, there is also the previously discussed production mode $q\bar{q} \rightarrow W^* \rightarrow W(\rightarrow \ell\nu)H$, which has been shown to be indistinguishable from SM background processes.⁶⁵

The Higgs boson can decay to the usual SM decay modes, as well as the invisible decay mode $H \rightarrow \nu_L \bar{\nu}_R$ that we have described previously. The SM modes $H \rightarrow b\bar{b}$ and $H \rightarrow WW^*$ are dominant. Since the invisible decay mode can only dominate at low Higgs boson masses $m_H < 160 \text{ GeV}$, we restrict our attention to this mass region and will not consider the $H \rightarrow WW^*$ decay mode. It should also be noted that it is difficult to detect the WW^* state. This is because the leptonic decay branching ratio is suppressed and the hadronic decay modes are dominated by background.

We consider the two Higgs boson decay modes, invisible and $b\bar{b}$, for the new process. The decay mode

$$q\bar{q}' \rightarrow W^* \rightarrow \ell^+ H(\rightarrow b\bar{b})\nu_R \quad (65)$$

suffers from large background. However, this channel allows the invariant mass of the Higgs boson to be reconstructed. The signature is $\ell b\bar{b}$ plus missing energy, where we will only consider $\ell = e$ or μ , because of the difficulty in reconstructing the different decay modes of the τ jet. We will assume the b jets can be tagged

by an experiment with an efficiency of about 50%, say. Two intrinsic SM processes dominate the background

$$q\bar{q}' \rightarrow W^* \rightarrow \bar{b}t[\rightarrow bW^+(\rightarrow \ell^+\nu)], \quad (66)$$

$$q\bar{q}' \rightarrow W^* \rightarrow W^+(\rightarrow \ell^+\nu)g(\rightarrow b\bar{b}). \quad (67)$$

Ref. 68 has shown, that even with a perfect detector, for $\delta = 3$, $M_D = 3.7$ TeV, $m_H = 115$ GeV, and 100 fb^{-1} of data, only eight events above a background of 10^5 can be obtained. Therefore it would be extremely difficult to use the $b\bar{b}$ mode to directly detect the signal at the LHC. However, a novel approach employing state-of-the-art jet reconstruction and decomposition techniques indicates that $H \rightarrow b\bar{b}$ is a promising search channel for a SM Higgs bosons around 120 GeV in mass.⁶⁶ A recent study by the ATLAS collaboration has confirmed the viability of the new technique.⁶⁷

Now consider the decay mode

$$q\bar{q}' \rightarrow W^* \rightarrow \ell^+ H(\rightarrow \nu_L \bar{\nu}_R) \nu_R. \quad (68)$$

The signature is $\ell = e, \mu$, or τ plus missing energy. For the τ , we will consider only the $\tau^+ \rightarrow \pi^+ \nu$ decay mode. So the resulting signatures are π^+ plus missing energy or ℓ^+ plus missing energy, where now $\ell = e$ or μ only. The major SM background is the Drell-Yan charged current process $q\bar{q}' \rightarrow W^* \rightarrow \ell^+ \nu$.

To search for an invisible decay mode, one can apply a set of cuts to enhance the signal to background and then look at the shape of the missing transverse energy spectrum. The procedure must be applied to the different mass hierarchy schemes separately since the relative numbers of each lepton type in the final state differ. Ref. 68 has shown that the $\ell^+ \cancel{E}_T$ and $\pi^+ \cancel{E}_T$ channels lead to similar significances. If M_D is about 5 TeV (for normal or inverted) or about 20 TeV (for degenerate) we may expect the significance to be in the range of $2 - 5 \sigma$.⁶⁸ If we strictly impose the constraints on $1/R$, we would expect a poor significance. However, we have pointed out previously that because of the dependence on the UV cut-off for $\delta = 3$, those constraints are uncertain to some extent. Therefore, in the event that the constraint on M_D is relaxed somewhat, we may expect to see a signal at the LHC. We may also expect to see a signal if we consider a model with bulk neutrinos in a subspace of extra dimensions, or asymmetric dimensions.

Neutrino oscillation data do not give the sign of Δm_{atm}^2 nor the absolute scale of the neutrino masses. Measuring the sign of Δm_{atm}^2 would determine directly whether the normal or the inverted mass hierarchy is realized in nature. Can we use the collider observables to distinguish between the normal, inverted, or degenerate mass schemes? We can define a lepton flavour asymmetry. Let $N(e + \cancel{E}_T)$ and $N(\mu + \cancel{E}_T)$ be the number of electron and muon signal events, respectively. Define

$$A_{\mu e} \equiv \frac{N(\mu + \cancel{E}_T) - N(e + \cancel{E}_T)}{N(\mu + \cancel{E}_T) + N(e + \cancel{E}_T)}. \quad (69)$$

From this asymmetry one can obtain

$$A_{\mu e} \sim \frac{\pm 0.5 \Delta m_{\text{atm}}^2}{2m_1^2 \pm 0.5 \Delta m_{\text{atm}}^2}, \quad (70)$$

where the upper sign is for the normal mass hierarchy and the lower sign is for the inverted mass hierarchy. Thus $A_{\mu e} > 0$ for the normal mass hierarchy and $A_{\mu e} < 0$ for the inverted mass hierarchy. For the inverted mass hierarchy, the smallest value that m_1 can take is 0.05 eV. Figure 18 shows the ideal situation with no experimental affects included. For small m_1 , there is excellent discrimination power to determine whether the normal or inverted mass hierarchy is realized. However, as m_1 is increased, the number of e , μ , and τ lepton events becomes approximately equal and the discriminating power diminishes. We might also be able to determine the absolute scale of the neutrino mass m_1 , but only if m_1^2 is not too large compared to Δm_{atm}^2 . The $\tau - e$ (or $\tau - \mu$) asymmetry does not add any additional information in probing the neutrino masses.

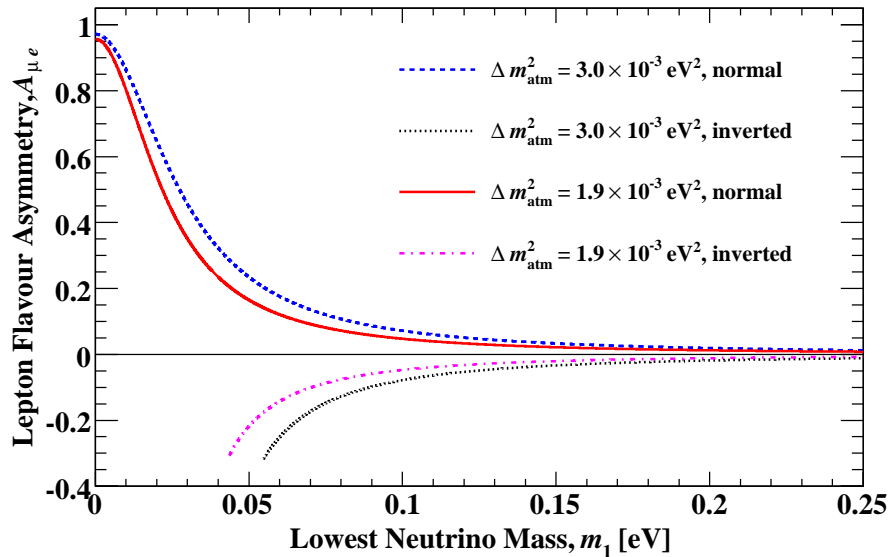


Fig. 18. Lepton flavour asymmetry $A_{\mu e}$ versus the lowest neutrino mass eigenstate m_1 for the existing bounds on atmospheric neutrino mixing. $A_{\mu e} > 0$ corresponds to the normal mass hierarchy, $A_{\mu e} < 0$ to the inverted mass hierarchy, and $A_{\mu e} \approx 0$ to the degenerate mass hierarchy

In summary, a signal of significance $2 - 5 \sigma$ for $\delta = 3$ and $M_D \sim 5$ TeV (normal or inverted mass hierarchies), or $M_D \sim 20$ TeV (degenerate mass scheme) could be obtained.⁶⁸ If a positive signal is found, the asymmetry in muon versus electron events could distinguish between the neutrino mass hierarchies and determine the absolute neutrino mass scale. The LHC might be a unique place to determine the hierarchy and mass scale as it is not available from neutrino oscillation experiments.

5. Summary

Singlet fermions in the bulk couple to the SM states on the brane as right-handed neutrinos with small couplings. The Yukawa couplings of the bulk fields are suppressed by the large volume of the extra dimensions. The interaction between the bulk fields and the brane fields generate Dirac mass terms between the neutrinos and all the KK modes of the bulk fields.

The effects of bulk neutrinos could be observed in charged Higgs boson decays. A clean sample of charged Higgs bosons would be needed to identify the model in which they are realized.

Observation of Higgs boson invisible decays in models of large extra dimensions could provide an opportunity to distinguish between the normal and inverted neutrino mass hierarchies, and to determine the absolute scale of the neutrino masses. Doing this requires measuring the asymmetry of the observed event numbers in the electrons and muons produced in association with the Higgs boson.

Observation of Higgs bosons in models with large extra dimensions will be difficult. This is due to the need to keep the dimensionless coupling constant low enough so that the effective theory is perturbative. However, models of asymmetric dimensions or bulk fermions living in a subspace of the extra dimensions allow a good chance to observe Higgs bosons at the LHC.

Acknowledgments

This work was supported in part by the Natural Sciences and Engineering Research Council of Canada.

Appendix A. Mass Mixing Normalisation Factor

In this appendix, we perform the sum over KK states in the normalisation factor of the mass mixing. From Eq. (31),

$$N^2 \approx 1 + \sum_n d_n \left(\frac{mR}{|\hat{n}|} \right)^2 = 1 + (mR)^2 \sum_n \frac{d_n}{n^2}. \quad (\text{A.1})$$

We have dropped the “hat” notation in the last expression. For generality, we will not require the number of extra dimensions that the bulk fermion propagates in δ_ν ,

to be the same as the number of extra dimensions of gravity δ . To obtain expressions for the case when the two spaces are the same take $\delta = \delta_\nu$.

For $\delta_\nu = 1$, the sum can be evaluated directly and the upper bound on the sum can be taken to infinity.

$$\begin{aligned}
 N^2 &= 1 + (mR)^2 \frac{\pi^2}{6} \\
 &= 1 + \left(\frac{m}{M_D}\right)^2 \left(\frac{\bar{M}_{\text{Pl}}}{M_D}\right)^{4/\delta} \frac{\pi^2}{6} \\
 &= 1 + \left(\frac{m}{M_D}\right)^2 \left(\frac{\bar{M}_{\text{Pl}}}{M_D}\right)^{2\delta_\nu/\delta} \left(\frac{\bar{M}_{\text{Pl}}}{M_D}\right)^{2/\delta} \frac{\pi^2}{6}, \tag{A.2}
 \end{aligned}$$

where Eq. (5) has been used to replace R in terms of M_D and \bar{M}_{Pl} in the second expression.

For $\delta > 1$, the infinite sum does not converge so we replace the sum by an integral over a sphere.

$$\sum_n d_n \rightarrow S_{\delta-1} n^{\delta-1} dn, \tag{A.3}$$

where $S_{\delta-1} = 2\pi^{\delta/2}/\Gamma(\delta/2)$. We have

$$N^2 \approx 1 + (mR)^2 S_{\delta-1} \int_1^{M_D R} n^{\delta-3} dn. \tag{A.4}$$

For $\delta_\nu = 2$,

$$\begin{aligned}
 N^2 &= 1 + (mR)^2 2\pi \ln(M_D R) \\
 &= 1 + \left(\frac{m}{M_D}\right)^2 \left(\frac{\bar{M}_{\text{Pl}}}{M_D}\right)^{4/\delta} 2\pi \ln\left(\frac{\bar{M}_{\text{Pl}}}{M_D}\right)^{2/\delta} \\
 &= 1 + \left(\frac{m}{M_D}\right)^2 \left(\frac{\bar{M}_{\text{Pl}}}{M_D}\right)^{2\delta_\nu/\delta} \frac{4\pi}{\delta} \ln\left(\frac{\bar{M}_{\text{Pl}}}{M_D}\right). \tag{A.5}
 \end{aligned}$$

For $\delta_\nu > 2$,

$$\begin{aligned}
 N^2 &\approx 1 + (mR)^2 \frac{2\pi^{\delta_\nu/2}}{\Gamma(\delta_\nu/2)} \frac{(M_D R)^{\delta_\nu-2}}{\delta_\nu-2} \\
 &= 1 + \left(\frac{m}{M_D}\right)^2 (M_D R)^{\delta_\nu} \frac{2\pi^{\delta_\nu/2}}{\Gamma(\delta_\nu/2)} \frac{1}{\delta_\nu-2} \\
 &= 1 + \left(\frac{m}{M_D}\right)^2 \left(\frac{\bar{M}_{\text{Pl}}}{M_D}\right)^{2\delta_\nu/\delta} \frac{2\pi^{\delta_\nu/2}}{\Gamma(\delta_\nu/2)} \frac{1}{\delta_\nu-2}. \tag{A.6}
 \end{aligned}$$

In the first line of above expression, we have made the approximation that the lower bound of integration can be taken to be zero.

Appendix B. Scalar Boson to Two-Fermion Decay Widths

The $1 \rightarrow 2$ decay width is

$$\Gamma = \frac{p}{8\pi M^2} |\mathcal{M}|^2, \quad (\text{B.1})$$

where the magnitude of either outgoing momentum in the boson rest frame is

$$p = \frac{M}{2} \sqrt{\left[1 - \left(\frac{m_1 + m_2}{M}\right)^2\right] \left[1 - \left(\frac{m_1 - m_2}{M}\right)^2\right]}. \quad (\text{B.2})$$

If $m_2 \ll m_1$ or $m_2 \ll M$ ($m_1 \equiv m$),

$$p \approx \frac{M}{2} \left[1 - \left(\frac{m}{M}\right)^2\right]. \quad (\text{B.3})$$

If $m_1 \ll M$ and $m_2 \ll M$,

$$p \approx \frac{M}{2}. \quad (\text{B.4})$$

The matrix element consists of a vertex factor times a spinor product

$$\mathcal{M} = y_\nu \mathcal{M}'. \quad (\text{B.5})$$

The spinor product for a signal polarization state is

$$\begin{aligned} \mathcal{M}' &= \bar{u}v = u^\dagger \gamma^0 v = \sqrt{(E_1 + m_1)(E_2 - m_2)} + \sqrt{(E_1 - m_1)(E_2 + m_2)}, \\ (\mathcal{M}')^2 &= 2ME_2 - 2m_2^2 - 2m_1m_2. \end{aligned} \quad (\text{B.6})$$

If $m_2 \ll M$,

$$\mathcal{M}' \approx \sqrt{2Mp}. \quad (\text{B.7})$$

If $m_1 \ll M$ and $m_2 \ll M$,

$$\mathcal{M}' \approx 2E = M. \quad (\text{B.8})$$

For fermions (not neutrinos), there will be two polarization states and hence the matrix element squared should be multiplied by a factor of two. For SM neutrinos this factor of two will be absent. Including the two polarization states, we have

$$\Gamma = \frac{y_\nu^2 M}{8\pi} \left[1 - \left(\frac{m}{M}\right)^2\right]^2, \quad (\text{B.9})$$

for $m_2 \ll M$.

$$\Gamma = \frac{y_\nu^2 M}{8\pi}, \quad (\text{B.10})$$

for $m_1 \ll M$ and $m_2 \ll M$.

Appendix B.1. SM Higgs Boson and MSSM Charged Higgs Boson Decay Widths

For the SM Higgs boson,

$$y_\nu = -i \frac{gm_f}{2m_W} = -i \frac{m_f}{v}. \quad (\text{B.11})$$

For $H^+ \rightarrow t\bar{b}$ in MSSM,

$$y_\nu = \frac{\sqrt{2}}{v} (m_t \cot \beta P_R + m_b \tan \beta P_L). \quad (\text{B.12})$$

For $H^+ \rightarrow \tau^+\nu$ in MSSM,

$$y_\nu = \frac{\sqrt{2}}{v} (m_\tau \tan \beta P_L). \quad (\text{B.13})$$

Consider $H^+ \rightarrow \tau_R^+\nu$ in MSSM. Using $y_\nu = \sqrt{2}(m_\tau/v) \tan \beta P_L$, $p = M/2$, and $\mathcal{M}' = M$ gives

$$\Gamma^{MSSM} = \frac{M}{8\pi} \left(\frac{m_\tau}{v} \right)^2 \tan^2 \beta. \quad (\text{B.14})$$

Appendix B.2. Large Extra Dimensions Decay Widths

Consider $H^+ \rightarrow \tau_R^+\nu$ in the model of bulk fermions in large extra dimensions. We separate the zero mode from the \hat{n} modes; $\Gamma = \sum_n \Gamma^{(n)} = \Gamma^{(0)} + \sum_{\hat{n}} \Gamma^{(\hat{n})}$. Using $y_\nu = \sqrt{2}(m_\tau/v) \tan \beta P_L$, $p_0 = M/2$, $p_{(\hat{n})} = (M/2)[1 - 1/M^2(n/R)^2]$, and $\mathcal{M}'_0 = M/N$, $\mathcal{M}'_{(\hat{n})} = (m_D R/n) \sqrt{2M p_{(\hat{n})}}/N$ gives

44 *Douglas M. Gingrich*

$$\begin{aligned}
 \Gamma &= \frac{\Gamma_{MSSM}}{N^2} \\
 &+ \frac{1}{8\pi M} \left[2 \left(\frac{m_\tau}{v} \right)^2 \tan^2 \beta \right] \frac{1}{N^2} \sum_n \left(\frac{m_D R}{n} \right)^2 2M \frac{M^2}{4} \left[1 - \frac{1}{M^2} \left(\frac{n}{R} \right)^2 \right]^2 \\
 &= \frac{\Gamma_{MSSM}}{N^2} + \frac{M}{8\pi} \left(\frac{m_\tau}{v} \right)^2 \tan^2 \beta \frac{1}{N^2} \left(\frac{m_D}{M} \right)^2 \sum_n M^2 \left(\frac{R}{n} \right)^2 \left[1 - \frac{1}{M^2} \left(\frac{n}{R} \right)^2 \right]^2 \\
 &= \frac{\Gamma_{MSSM}}{N^2} \left[1 + \left(\frac{m_D}{M} \right)^2 (MR)^\delta x_{\delta-2} \right] \\
 &= \frac{\Gamma_{MSSM}}{N^2} \left[1 + \left(\frac{m_D}{M_D} \right)^2 \left(\frac{M_{P1}}{M_D} \right)^2 \left(\frac{M}{M_D} \right)^{\delta-2} x_{\delta-2} \right]. \tag{B.15}
 \end{aligned}$$

See Appendix C for a calculation of $x_{\delta-2}$.

Consider $H^+ \rightarrow \tau_L^+ \nu_R$. Using $y_\nu = \sqrt{2}(m_D/v) \cot \beta P_R$, $p = (M/2)[1 - (1/M^2)(n/R)^2]$, and $\mathcal{M}' = \sqrt{2Mp}$ gives

$$\begin{aligned}
 \Gamma &= \frac{1}{8\pi M} \left[2 \left(\frac{m_D}{v} \right)^2 \cot^2 \beta \right] 2M \frac{M^2}{4} \sum_n \left[1 - \frac{1}{M^2} \left(\frac{n}{R} \right)^2 \right]^2 \\
 &= \frac{M}{8\pi} \left(\frac{m_D}{v} \right)^2 \cot^2 \beta (MR)^\delta x_\delta. \tag{B.16}
 \end{aligned}$$

See Appendix C for a calculation of x_δ .

Appendix C. Kaluza Klein Phase Space Sums

For bulk fermions, the masses of the KK states are not negligible, nor are the masses of the final two particles equal. Thus $[1 - (m/M)^2]^2$ with $m = n/R$ summed over the number of KK states is the quantity of interest in the decay width.

$$\begin{aligned}
 x_\delta &\equiv \sum_n \left[1 - \frac{1}{M^2} \left(\frac{n}{R} \right)^2 \right]^2 \\
 &= \sum_n \left[1 - \frac{2}{(MR)^2} n^2 + \frac{1}{(MR)^4} n^4 \right] \\
 &= \frac{2\pi^{\delta/2}}{\Gamma(\delta/2)} \int_0^{MR} \left[n^{\delta-1} - \frac{2}{(MR)^2} n^{\delta+1} + \frac{1}{(MR)^4} n^{\delta+3} \right] dn \\
 &= \frac{2\pi^{\delta/2}}{\Gamma(\delta/2)} \left[\frac{n^\delta}{\delta} - \frac{2n^{\delta+2}}{(MR)^2(\delta+2)} + \frac{n^{\delta+4}}{(MR)^4(\delta+4)} \right]_0^{MR} \\
 &= (MR)^\delta \frac{2\pi^{\delta/2}}{\Gamma(\delta/2)} \left(\frac{1}{\delta} - \frac{2}{\delta+2} + \frac{1}{\delta+4} \right). \tag{C.1}
 \end{aligned}$$

Also of interest is

$$\begin{aligned}
x_{\delta-2} &\equiv \sum_n M^2 \left(\frac{R}{n}\right)^2 \left[1 - \frac{1}{M^2} \left(\frac{n}{R}\right)^2\right]^2 \\
&= \sum_n \left[(MR)\frac{1}{n} - \frac{1}{(MR)}n\right]^2 \\
&= \sum_n \left[(MR)^2\frac{1}{n^2} - 2 + \frac{1}{(MR)^2}n^2\right] \\
&= \frac{2\pi^{\delta/2}}{\Gamma(\delta/2)} \int_0^{MR} \left[(MR)^2 n^{\delta-3} - 2n^{\delta-1} + \frac{1}{(MR)^2}n^{\delta+1}\right] dn \\
&= \frac{2\pi^{\delta/2}}{\Gamma(\delta/2)} \left[(MR)^2 \frac{(MR)^{\delta-2}}{\delta-2} - 2\frac{(MR)^\delta}{\delta} + \frac{1}{(MR)^2} \frac{(MR)^{\delta+2}}{\delta+2}\right] \\
&= (MR)^\delta \frac{2\pi^{\delta/2}}{\Gamma(\delta/2)} \left(\frac{1}{\delta-2} - \frac{2}{\delta} + \frac{1}{\delta+2}\right). \tag{C.2}
\end{aligned}$$

References

1. Y. Fukuda *et al.*, *Phys. Rev. Lett.* **81**, 1562 (1998).
2. Y. Fukuda *et al.*, *Phys. Rev. Lett.* **86**, 5651 (2001).
3. Q.R. Ahmed *et al.*, *Phys. Rev. Lett.* **87**, 071301 (2001).
4. Q.R. Ahmed *et al.*, *Phys. Rev. Lett.* **89**, 011301 (2002).
5. Q.R. Ahmed *et al.*, *Phys. Rev. Lett.* **89**, 011302 (2002).
6. K. Eguchi *et al.*, *Phys. Rev. Lett.* **90**, 021802 (2003).
7. S.N. Ahmed *et al.*, *Phys. Rev. Lett.* **92**, 181301 (2004).
8. Y. Ashie *et al.*, *Phys. Rev. Lett.* **93**, 101801 (2004).
9. T. Araki *et al.*, *Phys. Rev. Lett.* **94**, 081801 (2005).
10. Y. Ashie *et al.*, *Phys. Rev. D* **71**, 112005 (2005).
11. B. Aharmim *et al.*, *Phys. Rev. C* **72**, 055502 (2005).
12. N. Arkani-Hamed, S. Dimopoulos and G. Dvali, *Phys. Lett. B* **429**, 263 (1998).
13. I. Antoniadis, N. Arkani-Hamed, S. Dimopoulos and G. Dvali, *Phys. Lett. B* **436**, 257 (1998).
14. N. Arkani-Hamed, S. Dimopoulos and G. Dvali, *Phys. Rev. D* **59**, 086004 (1999).
15. K.R. Dienes, E. Dudas and T. Gherghetta, *Nucl. Phys. B* **557**, 25 (1999).
16. G. Dvali and A.Y. Smirnov, *Nucl. Phys. B* **563**, 63 (1999).
17. N. Arkani-Hamed, S. Dimopoulos, G. Dvali and J. March-Russell, *Phys. Rev. D* **65**, 024032 (2001).
18. A. Aguilar *et al.*, *Phys. Rev. D* **64**, 112007 (2001).
19. R.N. Mohapatra and A. Pérez-Lorenzana, *Nucl. Phys. B* **593**, 451 (2001).
20. C. Amsler *et al.*, *Phys. Lett. B* **667** (2008).
21. D.J. Kapner, T.S. Cook, E.G. Adelberger, J.H. Gundlach, B.R. Heckel, C.D. Hoyle and H.E. Swanson, *Phys. Rev. Lett.* **98**, 021101 (2007).
22. H. Davoudiasl, P. Langacker and M. Perelstein, *Phys. Rev. D* **65**, 105015 (2002).
23. K.R. Dienes and I. Sarcevic, *Phys. Lett. B* **500**, 133 (2001).
24. C.S. Lam and J.N. Ng, *Phys. Rev. D* **64**, 113006 (2001).
25. K.R. Dienes and S. Hossenfelder, *Phys. Rev. D* **74**, 065013 (2006).
26. J. Matias and C.P. Burgess, *J. High Energy Phys.* **0509**, 052 (2005).
27. Q.-H. Cao, S. Gopalakrishna and C.-P. Yuan, *Phys. Rev. D* **69**, 115003 (2004).

46 *Douglas M. Gingrich*

28. B. Pontecorvo, *JETP* **7**, 172 (1958).
29. B. Pontecorvo, *JETP* **26**, 984 (1968).
30. Z. Maki, M. Nakagawa and S. Sakata, *Prog. Theor. Phys.* **28**, 870 (1962).
31. M. Apollonio *et al.*, *Phys. Lett. B* **466**, 415 (1999).
32. K. Agashe and G.-H. Wu, *Phys. Lett. B* **498**, 230 (2001).
33. K.R. Dienes, *Phys. Rev. Lett.* **88**, 011601 (2002).
34. K.R. Dienes and A. Mafi, *Phys. Rev. Lett.* **88**, 111602 (2002).
35. K.R. Dienes and A. Mafi, *Phys. Rev. Lett.* **89**, 171602 (2002).
36. G.C. McLaughlin and J.N. Ng, *Phys. Lett. B* **493**, 88 (2000).
37. G.C. McLaughlin and J.N. Ng, *Phys. Rev. D* **63**, 053002 (2001).
38. A. de Gouvêa, G.F. Giudice, A. Strumia and K. Tobe, *Nucl. Phys. B* **623**, 395 (2002).
39. A. Ioannian and A. Pilaftsis, *Phys. Rev. D* **62**, 066001 (2000).
40. K. Agashe, N.G. Deshpande and G.-H. Wu, *Phys. Lett. B* **489**, 367 (2000).
41. N.G. Deshpande and D.K. Ghosh, *Phys. Lett. B* **567**, 235 (2003).
42. K.N. Abazajian, G.M. Fuller and M. Patel, *Phys. Rev. Lett.* **90**, 061301 (2003).
43. R. Barbieri, P. Creminelli and A. Strumia, *Nucl. Phys. B* **585**, 28 (2000).
44. G. Cacciapaglia, M. Cirelli and A. Romanino, *Phys. Rev. D* **68**, 033013 (2003).
45. H.S. Goh and R.N. Mohapatra, *Phys. Rev. D* **65**, 085018 (2002).
46. A.E. Faraggi and M. Pospelov, *Phys. Lett. B* **458**, 237 (1999).
47. Z-z. Xing, *Int. J. Mod. Phys. A* **23** 4255 (2008).
48. Z-z. Xing, “Naturalness and Testability of TeV Seesaw Mechanisms,” arXiv:0905.3903v2 [hep-ph].
49. F. del Aguila and J.A. Aguilar-Saavedra, *Nucl. Phys. B* **813**, 22 (2009).
50. A. Atre, T. Han, S. Pascoli and B. Zhang, *J. High Energy Phys.* **0905**, 030 (2009).
51. ATLAS Collaboration, “Expected Performance of the ATLAS Experiment, Detector, Trigger and Physics,” CERN-OPEN-2008-020; arXiv:0901.0512v3 [hep-ex].
52. The TEVNPA Working Group for the CDF and DØ Collaborations, “Combined CDF and DØ Upper Limits on Standard Model Higgs-Boson Production with up to 4.2 fb^{-1} of Data,” arXiv:0903.4001v1 [hep-ex].
53. T. Plehn, *Phys. Rev. D* **67**, 014018 (2003).
54. E. Boos and T. Plehn, *Phys. Rev. D* **69**, 094005 (2004).
55. N. Kidonakis, *J. High Energy Phys.* **0505**, 011 (2005).
56. N. Kidonakis, “Higher order corrections to H^\pm production,” arXiv:0811.4757v1 [hep-ph].
57. S. Dittmaier, M. Krämer, M. Spira and M. Walser, “Charged-Higgs-boson production at the LHC: NLO supersymmetric QCD corrections,” arXiv:0906.2648v1 [hep-ph].
58. J. Alwall and J. Rathsman, *J. High Energy Phys.* **0412**, 050 (2004).
59. J. Alwall, “MATCHIG: A program for matching charged Higgs boson production at hadron colliders,” arXiv:hep-ph/0503124v1.
60. A. Djouadi, J. Kalinowski and M. Spira, *Comp. Phys. Com.* **108**, 56-74 (1998).
61. K.A. Assamagan and A. Deandrea, *Phys. Rev. D* **65**, 076006 (2002).
62. B. Mohn, M. Flechl and J. Alwall, “ATLAS Discovery Potential for the Charged Higgs Boson in $H^\pm \rightarrow \tau^\pm \nu_\tau$ Decays,” *ATL-PHYS-PUB-2007-006* (2007).
63. S. Raychaudhuri and D.P. Roy, *Phys. Rev. D* **52**, 1556 (1995).
64. S.P. Martin and J.D. Wells, *Phys. Rev. D* **60**, 035006 (1999).
65. R.M. Godbole, M. Guchait, K. Mazumdar, S. Moretti and D.P. Roy, *Phys. Lett. B* **571**, 184 (2003).
66. J.M. Butterworth, A.R. Davison, M. Rubin and G.P. Salam, *Phys. Rev. Lett.* **100**, 242001 (2008).
67. ATLAS Collaboration, “ATLAS Sensitivity to the Standard Model Higgs in the HW

Signatures of Singlet Neutrinos in Large Extra Dimensions at the LHC 47

and HZ Channels at High Transverse Momenta,” *ATL-COM-PHYS-2009-245*, *ATL-COM-PHYS-2009-345*.

68. Q.-H. Cao, S. Gopalakrishna and C.-P. Yuan, *Phys. Rev. D* **70**, 075020 (2004).